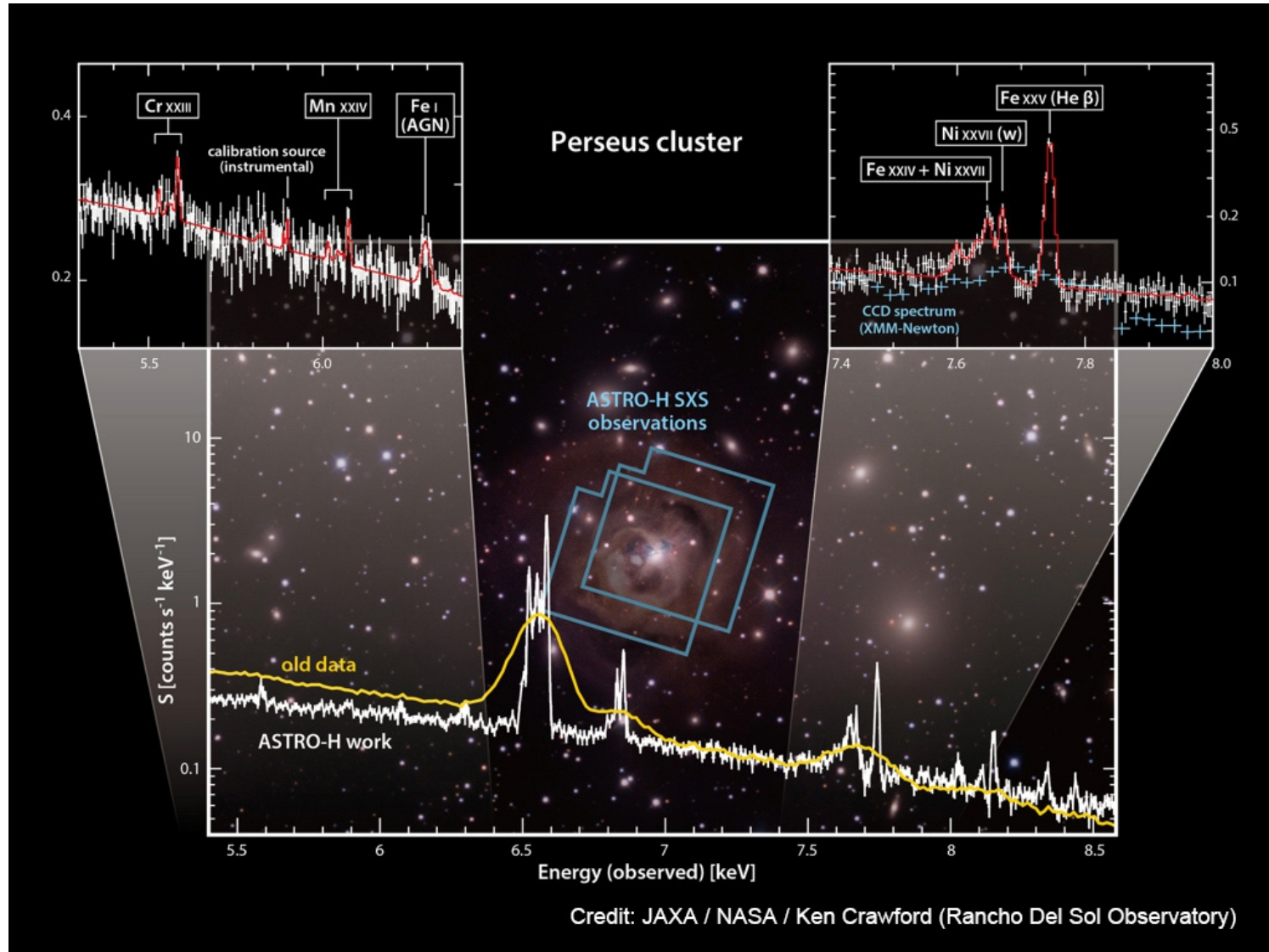


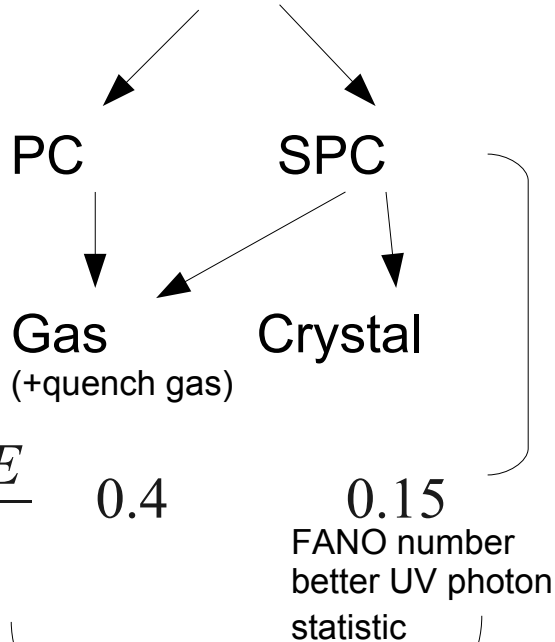
The Universe in X-rays: Lecture 4: High energy resolution



Agata Róžańska, fall semester, 2022/23

Summary after 1st and 2nd lecture:

1st Detectors:



**Bkgr. rejection, time res.,
det. lifetime.**

**Collimator,
anticoincidence system.**

2nd Imaging and X-ray optics:

MWPC, MWSPC (MultiWire)

- position on A_{det}
- ”crude” image

Mechanical collimators, MC:

- to restrict FOV
- position on A_{det}
- scanning – slat collimators

Coded Masks:

- spatial information
- image convolved with the mask pattern
- numerical technique to deconvolve the observed pattern

X-rays – reflection:

- total external reflection depends on E
- and on polarization (Fresnel's Eq.)

X-rays – imaging:

- scattering
- Wolter's Mirrors
- Abbe's sine condition works only for on-axis source
- off-axis source are always blurred

Point Spread Function:

- light gets blurred as it passes through the instrument
- image cannot be better than the PSF.

Summary after 3th lecture:

3rd X-ray CCDs:

- in the focus of imaging optics,
- single photon counting mode,
- used in largest X-ray telescopes ever build.

Why BI (back illuminated) CCD has less noise from particles?

Fully depleted CCDs:

- less amount of donors or acceptors increases depleted zone available for X-rays.

Back-illuminated CCDs:

- low energy X-rays are not lost in gate structures and filters,
- wider depleted zone.

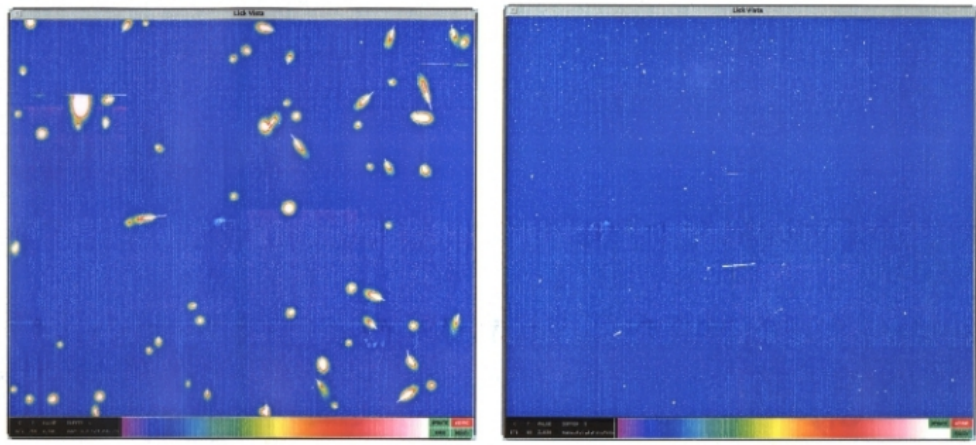
Charge transfer:

- three gates define one pixel,
- readout sequences,
- Pulse Height Amplitude.

Energy resolution:

- quantum efficiency
- noise – dark current

First Readout of ACIS CCDs



S2 = w182c4r

S3 = w134c4r

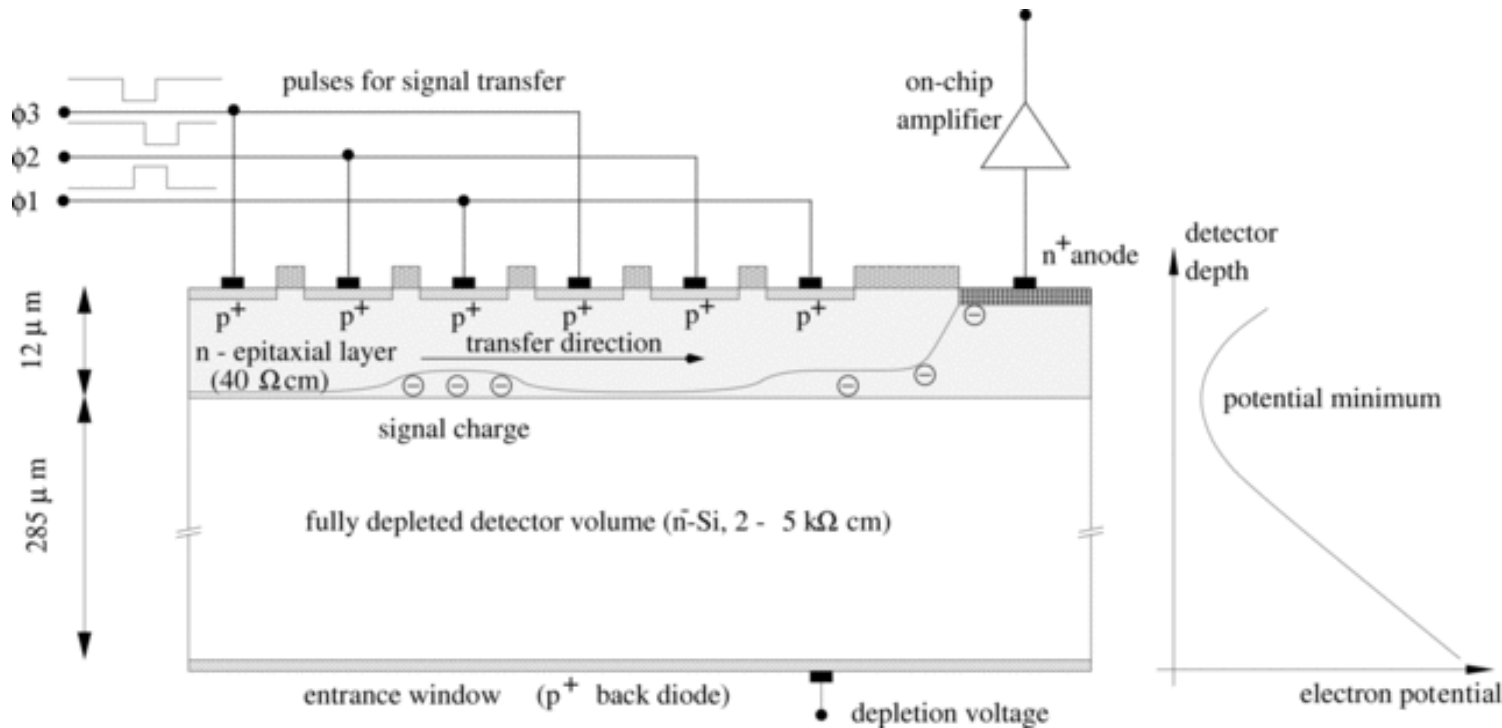
Front-illuminated CCD

Back-illuminated CCD

- Particle events produce large blooms on FI CCD, not on fully-depleted BI CCD
- Background rejection efficiency much higher for FI CCD

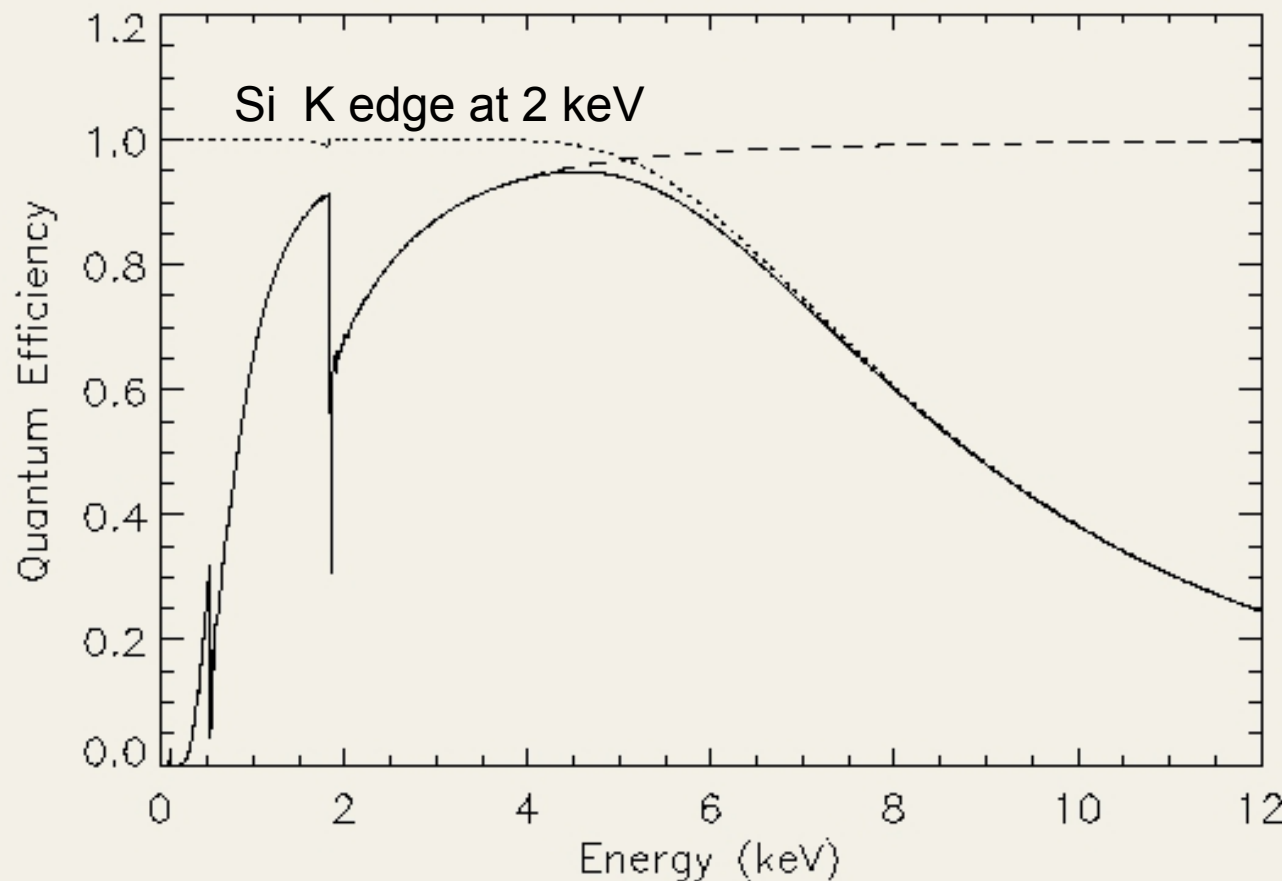
CCD – developed for X-rays:

50 μm and up for X-rays **back illuminated CCDs**



An additional negative voltage $\sim 150\text{ V}$, on the p⁺ back diode shifts the potential minimum for electrons out from the center towards the surface containing the pixel structure.

CCD Quantum Efficiency



Transmission
through deadlayers
(channel stops, gates,
oxide layers)

$$T = \prod_i e^{-\mu_i t_i}$$

Absorption in
depleted region

$$A = 1 - e^{-\mu_{Si} d}$$

μ = linear absorption coefficient
 t = thickness of deadlayer
 d = depletion depth

$$QE = (1 - e^{-\mu_{Si} d}) \prod_i e^{-\mu_i t_i}$$

Fully-Depleted, Back-Illuminated Charge-Coupled Devices Fabricated on High-Resistivity Silicon

Stephen E. Holland, Donald E. Groom, Nick P. Palaio, Richard J. Stover, Mingzhi Wei

Abstract— Charge-coupled devices (CCD's) have been fabricated on high-resistivity, n-type silicon. The resistivity, on the order of $10,000 \Omega\text{-cm}$, allows for depletion depths of several hundred microns. Fully-depleted, back-illuminated operation is achieved by the application of a bias voltage to a ohmic contact on the wafer back side consisting of a thin in-situ doped polycrystalline silicon layer capped by indium tin oxide and silicon dioxide. This thin contact allows for good short wavelength response, while the relatively large depleted thickness results in good near-infrared response.

Keywords— Charge-coupled device, back illuminated, fully depleted, high-resistivity silicon.

I. INTRODUCTION

THE large focal planes at astronomical telescopes require high quantum efficiency (QE), large format charge-coupled device (CCD) detectors. In order to achieve high QE, the standard scientific CCD is thinned and back illuminated [1]. Thinning is required because the relatively low resistivity silicon used to fabricate scientific CCD's limits the depth of the depletion region. In order to minimize field-free regions with resulting degradation in spatial resolution, the typical scientific CCD is thinned to about $20 \mu\text{m}$. This process degrades red and near-infrared response due to the rapid increase in absorption length in silicon at long wavelengths. In addition, fringing patterns due to multiply-reflected light are observed in uniformly-illuminated images taken at near-infrared wavelengths where the absorption length exceeds the CCD thickness. The CCD described in this work achieves high

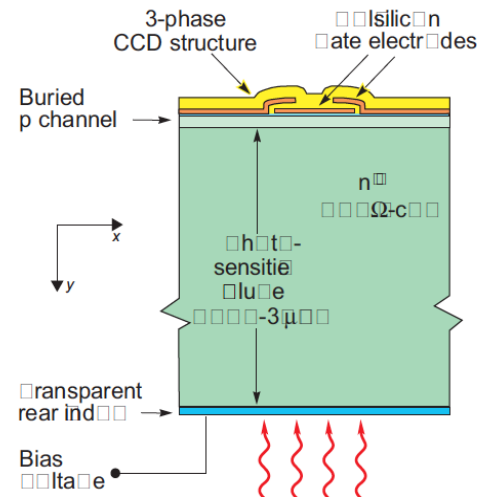


Fig. 1. Cross-sectional diagram of the CCD described in this work. The actual implementation of the substrate bias voltage connection is described in Section III.

II. BACKGROUND

Scientific CCD's are typically used in applications requiring low level light detection. Hence dark current, noise and quantum efficiency are of primary importance. For astronomy applications the CCD's are often cooled to -120°C to -150°C to minimize dark current. In addition read-out rates are relatively slow, typically 20–50 kpixels/sec, to minimize read noise [1]. The signal to noise ratio is further increased by the use of back illumination with correspondingly high quantum efficiency. Large format sensors are commonly used, and high charge transfer efficiency (CTE)

Fully-Depleted, Back-Illuminated Charge-Coupled Devices Fabricated on High-Resistivity Silicon

Stephen E. Holland, Donald E. Groom, Nick P. Palaio, Richard J. Stover, Mingzhi Wei

Abs
ricate
on th
sever
opera
a ohn
in-situ
tin ox
good
deplet
Key
deplet

In addition, a thick CCD reduces fringing [21]. In thinned CCD's fringing arises due to multiple reflections at long wavelengths when the absorption length of the incident light is greater than the CCD thickness. Fringing as well as the loss of QE limits the usefulness of scientific CCD's at long wavelengths.

THE large focal planes at astronomical telescopes require high quantum efficiency (QE), large format charge-coupled device (CCD) detectors. In order to achieve high QE, the standard scientific CCD is thinned and back illuminated [1]. Thinning is required because the relatively low resistivity silicon used to fabricate scientific CCD's limits the depth of the depletion region. In order to minimize field-free regions with resulting degradation in spatial resolution, the typical scientific CCD is thinned to about 20 μm . This process degrades red and near-infrared response due to the rapid increase in absorption length in silicon at long wavelengths. In addition, fringing patterns due to multiply-reflected light are observed in uniformly-illuminated images taken at near-infrared wavelengths where the absorption length exceeds the CCD thickness. The CCD described in this work achieves high

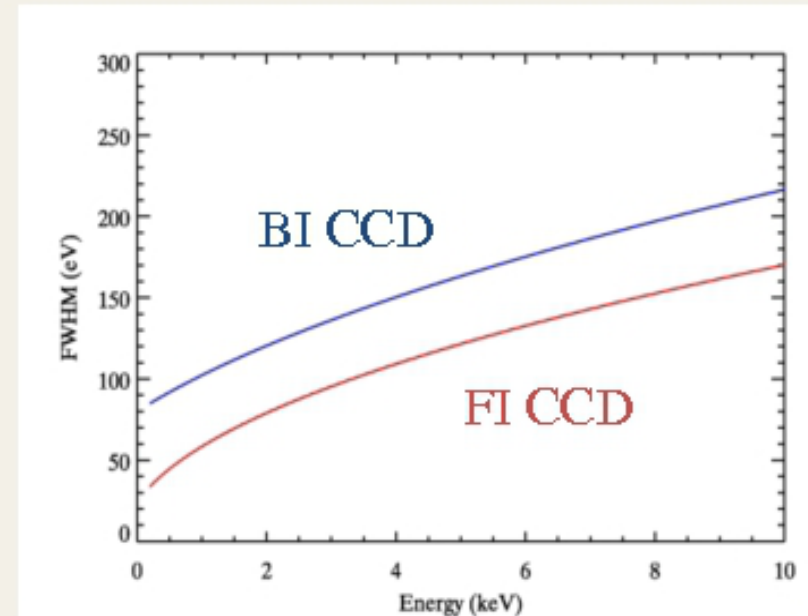
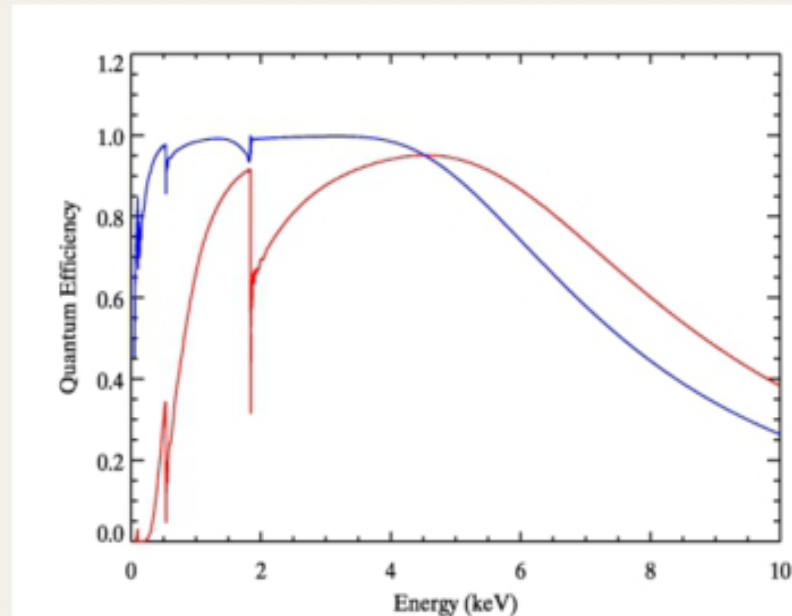
Fig. 1. Cross-sectional diagram of the CCD described in this work. The actual implementation of the substrate bias voltage connection is described in Section III.

II. BACKGROUND

Scientific CCD's are typically used in applications requiring low level light detection. Hence dark current, noise and quantum efficiency are of primary importance. For astronomy applications the CCD's are often cooled to -120°C to -150°C to minimize dark current. In addition read-out rates are relatively slow, typically 20–50 kpixels/sec, to minimize read noise [1]. The signal to noise ratio is further increased by the use of back illumination with correspondingly high quantum efficiency. Large format sensors are commonly used, and high charge transfer efficiency (CTE)

QE

Back-illuminated CCDs



- Front-illuminated CCD, reversed and thinned
- Gate structures and channel stops are not dead layers
- Thinner dead layers \Rightarrow higher low-E QE
- Thinner active region \Rightarrow lower high-E QE
 - Not always true, XMM EPIC-pn has excellent high-E QE
- Increased noise, charge transfer inefficiency \Rightarrow higher FWHM
 - Technology is maturing, Suzaku XIS BI quite good FWHM

Limitations of CCDs:

Quantum Efficiency depends E , and on the size of depletion zone. **The depleted device thickness, d** can be increased by using silicon with small donor concentration in n-type material. Maximum available **$d = 800 \mu\text{m}$** .

Ionization statistic depends on **Fano Factor $F=0.12$** for Si. Only 30% of incident energy is converted into $e^- h^+$ pairs. Equivalent noise charge contribution is given by:

$$ENC_{fano}^2 = \frac{E F}{w}, \quad \text{where: } w=3.7 \text{ eV, } E - \text{energy}$$

Charge transfer noise – electrons are transferred over many pixels. Charges left behinds form backward flow similar to signal leakage current.

$$ENC_{trans}^2 \simeq \frac{E}{w} (1 - CTE) N_{trans},$$

where N_{trans} – number of pixel transfers
CTE – charge transfer efficiency
CTE of the order of 10^{-5}

Electronic noise – readout noise has three components:

$$ENC_{el}^2$$

read node capacitance

low frequency noise

parallel noise (leakage current + normal current)

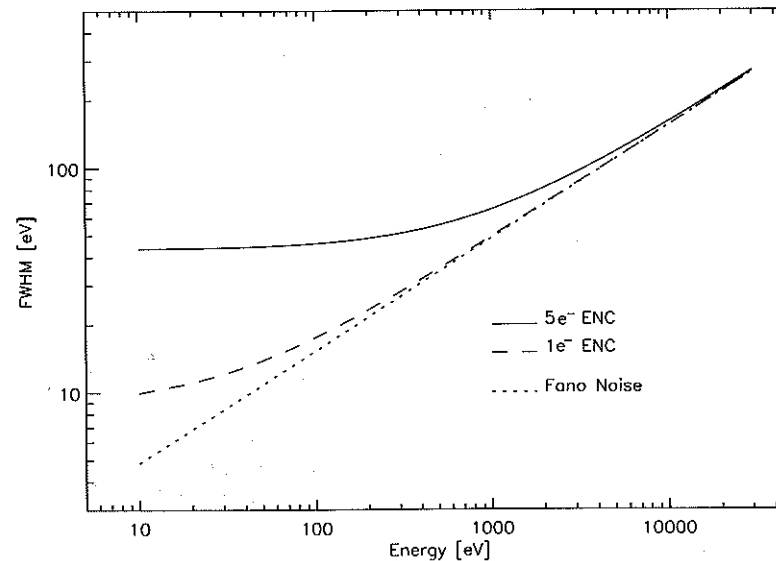


Fig. 7.8 Energy resolution as a function of the photon energy. The Fano noise is taken into account as well as a $5 e^-$ and $1 e^-$ electronic equivalent noise charge (ENC_{el}), respectively [22]

$$ENC_{tot}^2 = ENC_{el}^2 + ENC_{fano}^2 + ENC_{trans}^2 + \dots$$

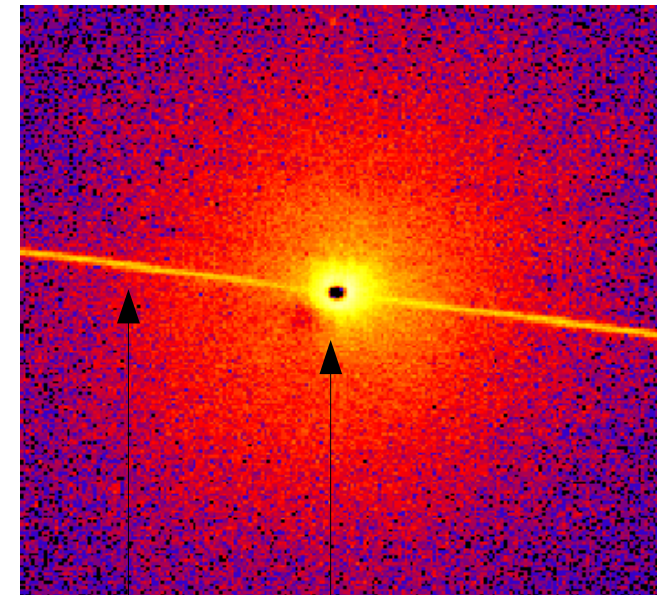
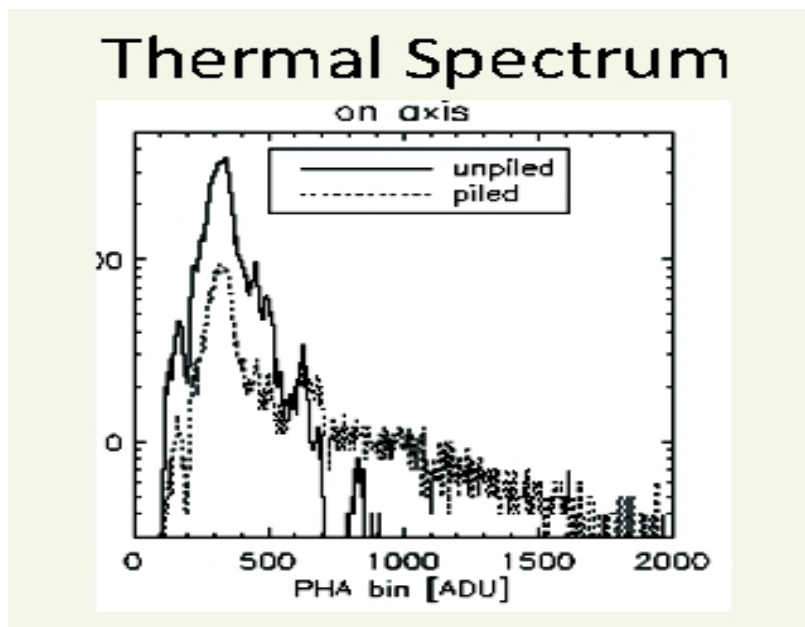
State of art pn CCD – $2e^-$ of el. noise and speed $10 \text{ pix}/\mu\text{s}$.

Detector features in CCD:

Photon pileup – two or more photons interact within a few pixels before the image is readout, the event finding algorithm may regard them as a single event.

Pileup makes:

- *higher inferred energy,*
- *piled event exceeds on-board spacecraft threshold (15 keV), it is rejected by spacecraft software – **pileup hole, PSF distortion,***
- ***readout streak,** photons interact while image is transferred*
- *spectral hardening of continuum sources,*



readout streak *pileup hole*

To reduce pileup:

- correcting data is possible but complicated,
- best to set up observations to minimize pileup,
- short time of exposure for sensitive CCD – XMM-Newton.

Diez Trigo + 2010

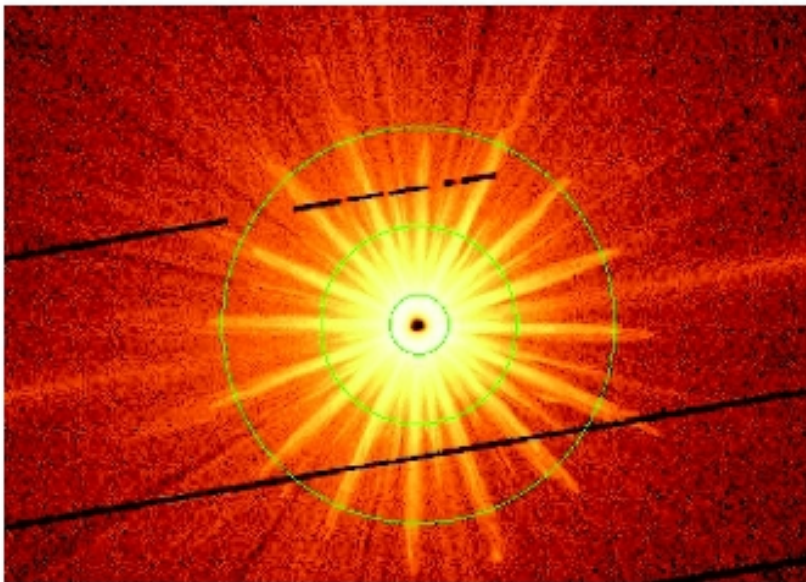


Figure 1. MOS1 image, with the black centre showing the extreme pile-up. The circles have radii of 18, 60 and 120 arcsec from the centre. We extract spectra from single events only from 0 to 120, 18 to 120, 60 to 120 and (not shown) 90 to 120 arcsec regions.

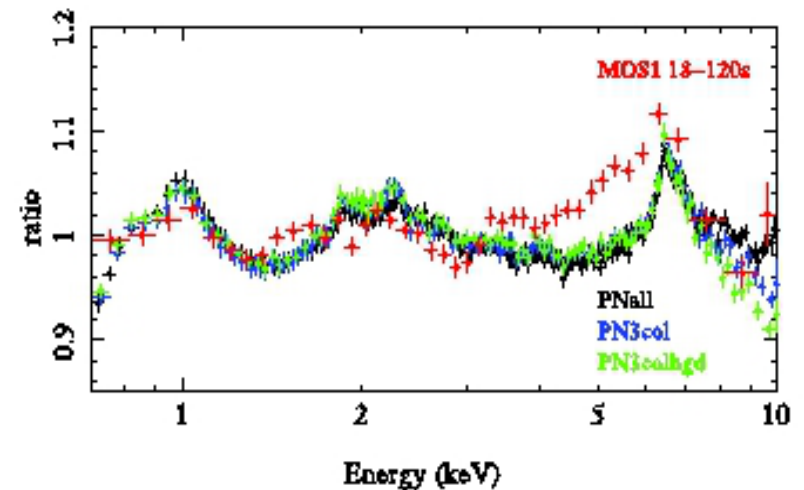


Figure 5. Ratio of PNall (black) to its best-fitting continuum model, excluding the 4–7 keV region. The blue and green points show the same model ratioed to the PN3col and PN3colbgd spectra. All these PN spectra are very similar except at the highest energies, where PN3colbgd (green) is steeper than PN3col (blue), which is steeper than PNall (black). We also show the MOS1 18–120s spectrum ratioed to its own best-fitting continuum model as in Fig. 4. The line profile is significantly broader in the piled-up MOS data than in any of the PN spectra.

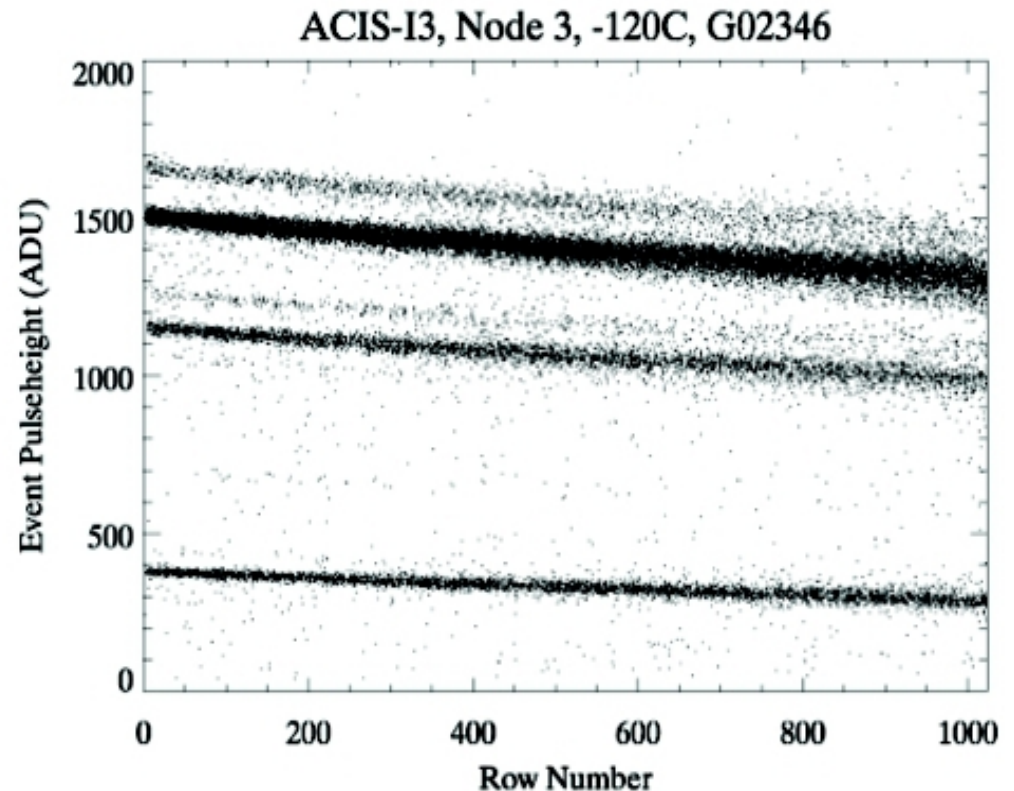
Charge transfer inefficiency : caused by radiation damage or manufacturing defects.

Leads to:

- *position dependent gain,*
- *spectral resolution degradation*
- *position dependent QE.*

Mitigation techniques:

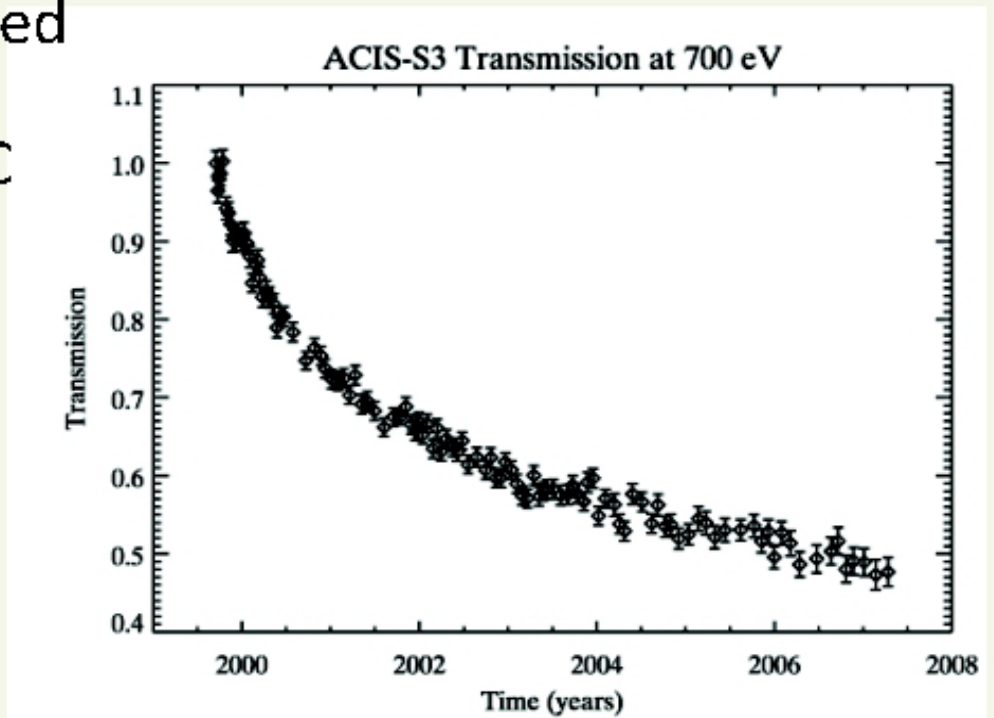
- *lower temperature,*
- *move target closer to readout,*
- *controlled charge injection (Suzaku XIS),*
- *specialized software tools.*



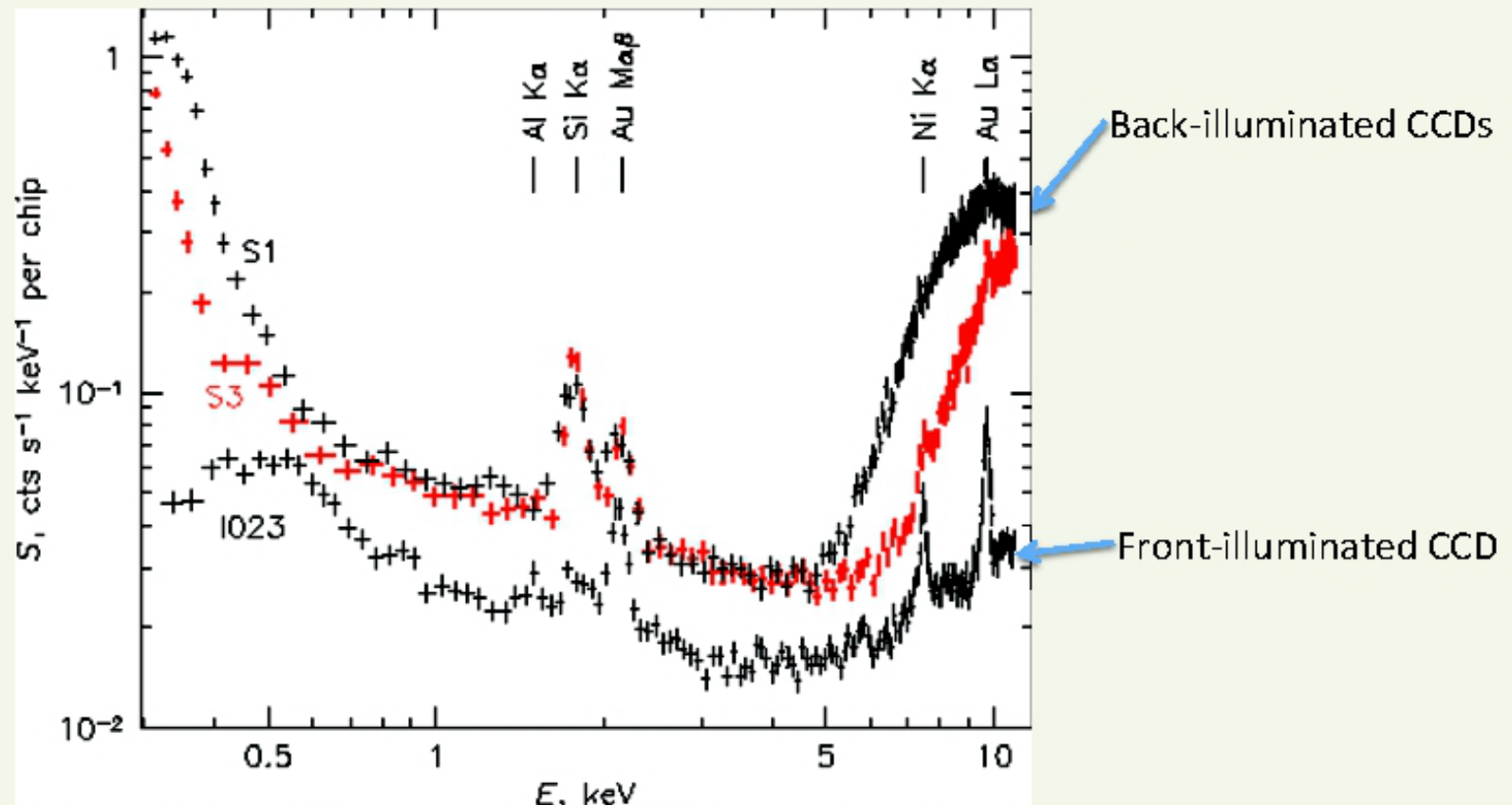
transfer direction

Contamination

- For best performance (reduced dark current and CTI), CCDs must be operated cold (-60°C to -120°C)
- Coldest surface, danger of accumulating contamination
- Contamination acts as an additional absorbing layer
- Can be important at low energies ($< 1\text{ keV}$)
- Important for Chandra ACIS, XMM RGS, Suzaku XIS, others?



Particle Background Spectrum



- ACIS in stowed position, no sky photons, standard grade filter
- Fluorescent lines from spacecraft materials plus continuum
- Grade filter less effective for back-illuminated CCDs, higher background rates

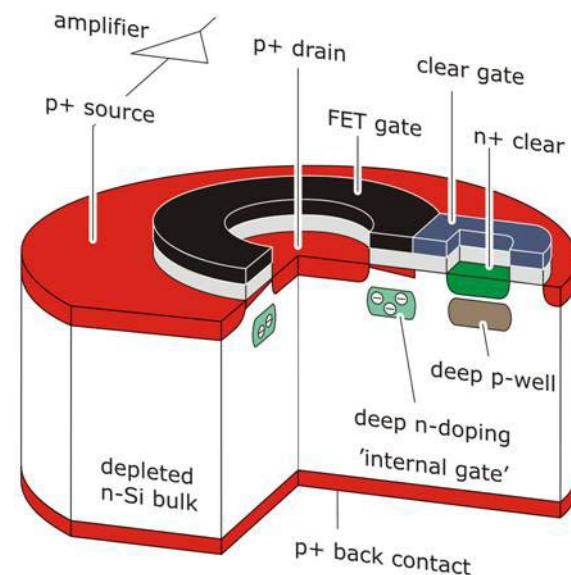
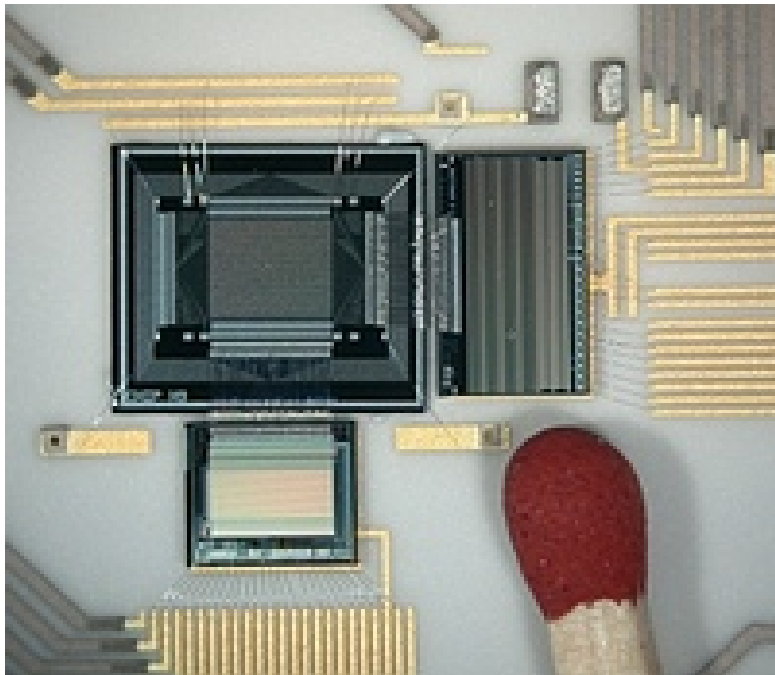
(From Chandra Proposer's Observatory Guide)

Active Pixel Sensor:

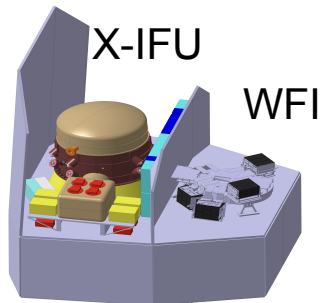
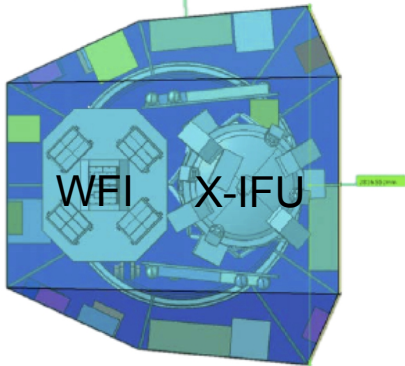
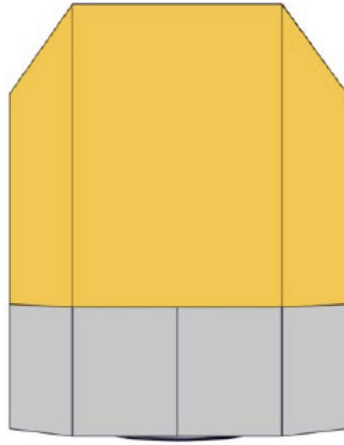
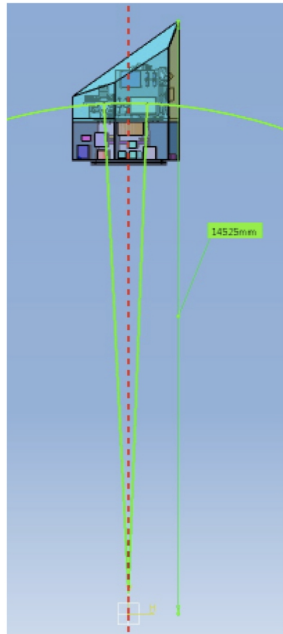
The weakness of CCDs is long transfer of signal charges parallel to the detector surface in large sensors up to several centimeter.

DEPFET – concept of **Active Pixel Sensor** – detector and amplifying element at the same time.

1024 x 1024 pixels with a pixel size **75 x 75 μm** .



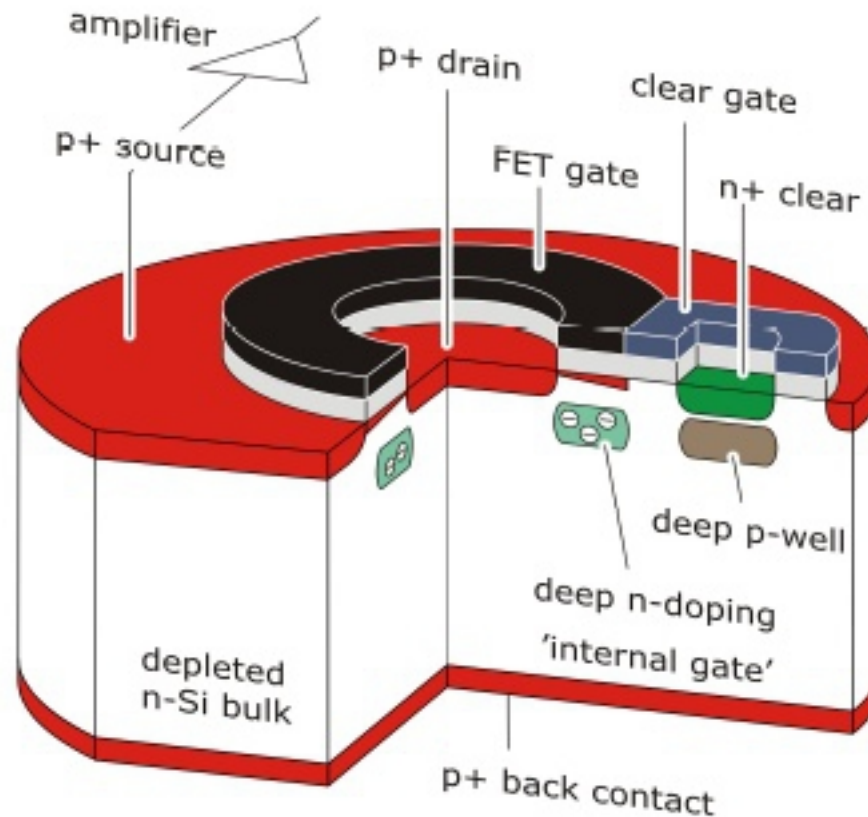
Athena X-ray Observatory



- L2 orbit, Ariane 64,
- 2032-33 yr
- Mass ~ 7100 kg
- Power ~ 10000 W
- > 4 year mission, 10+ yr
- 12 meters long, ESA L2 mission
- Budged < 1050 M Euro



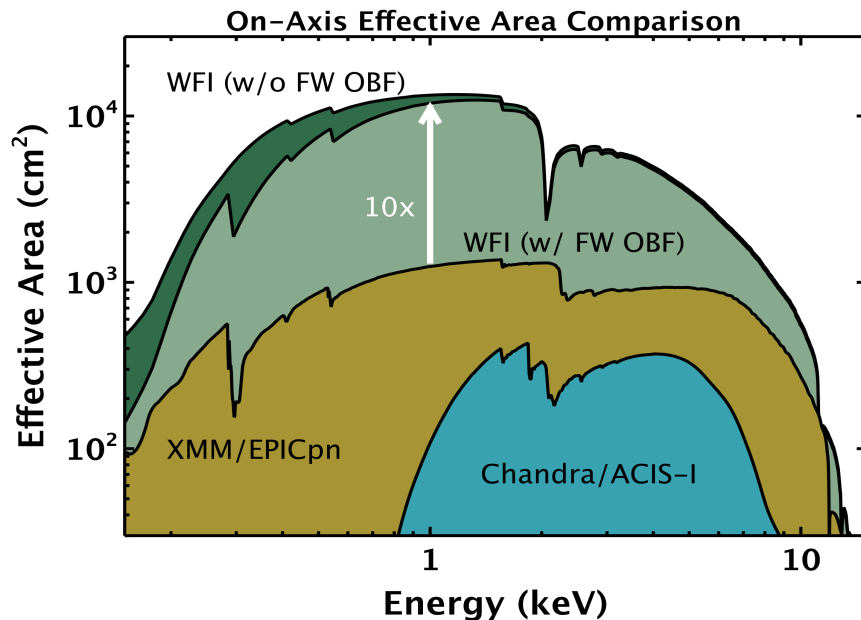
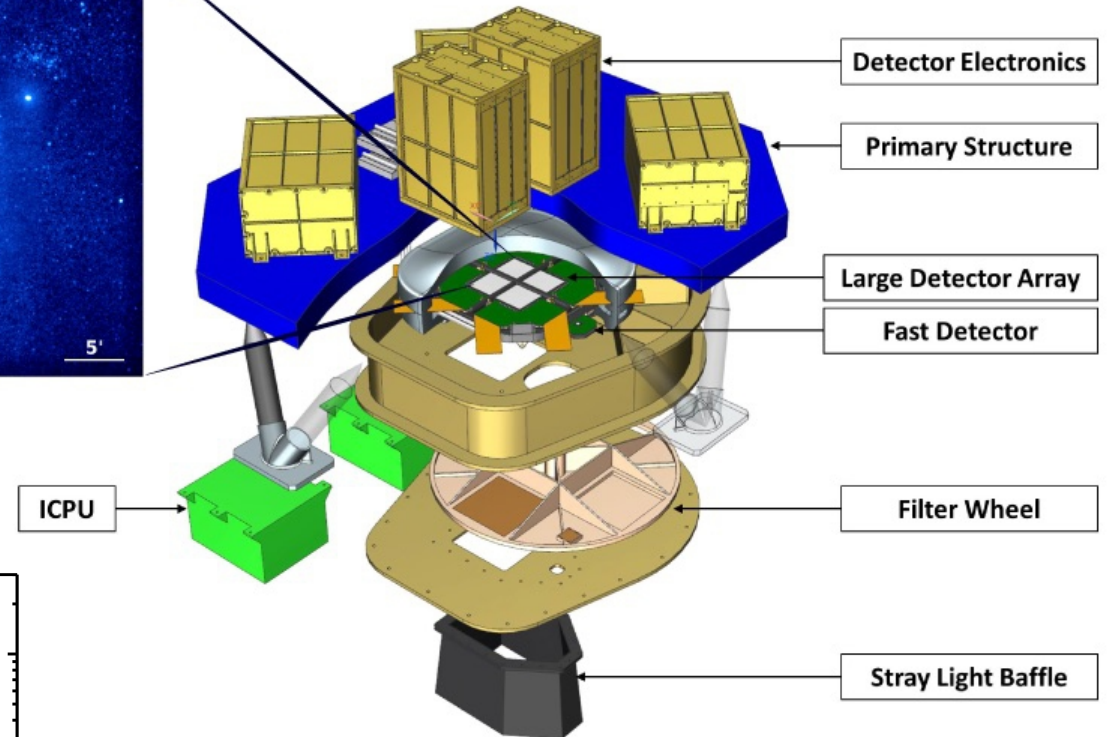
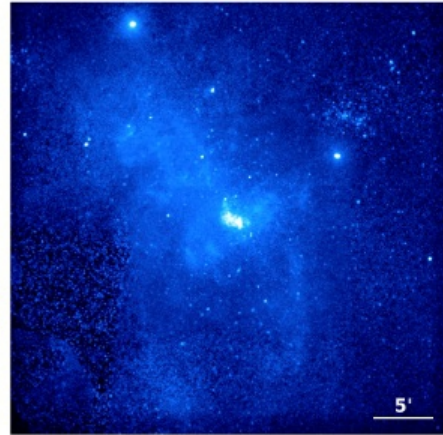
WFI – 0.1-15. keV is an array of Si-based DePFET – Depleted P-channel Field Effect Transistor - Active Pixel Sensor (APS)



$$\Delta E = 150 @ 6 \text{ keV}$$

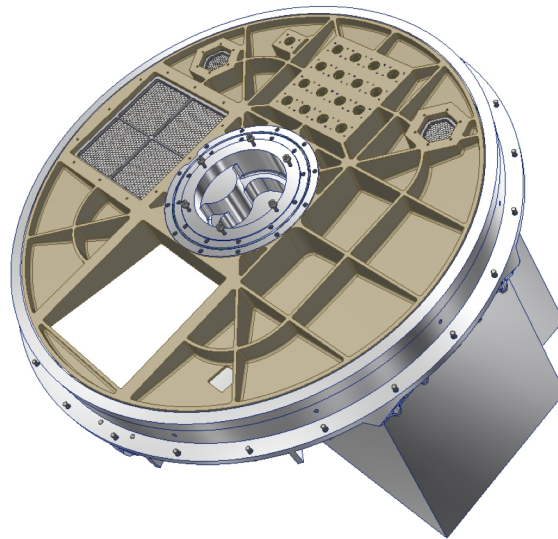
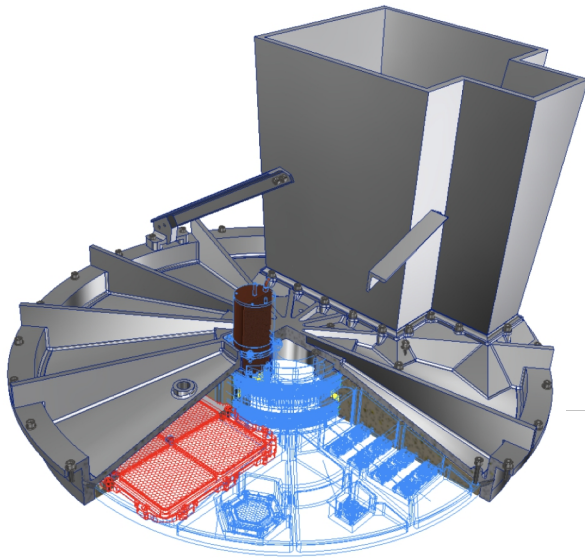
The DePFET is a combined detector-amplifier structure. Here, incident X-ray photons interact with the Si bulk material, and the resulting electron-hole pairs are separated.

256x256 pixels construct wide FoV 40' x 40' and will in particular allow high-time resolution observations of bright X-ray sources. With a readout time of 8 μ s in window mode and a count rate capability of >1 Crab with 80% throughput.



Poland for WFI, CBK and CAMK PAN

- Filter Wheel Assembly 632x64 mm
- Baffle - 675x430 mm
- PDU + 2 el. subsystems



CHANDRA Deep Field South, 100 ks

High resolution spectroscopy:

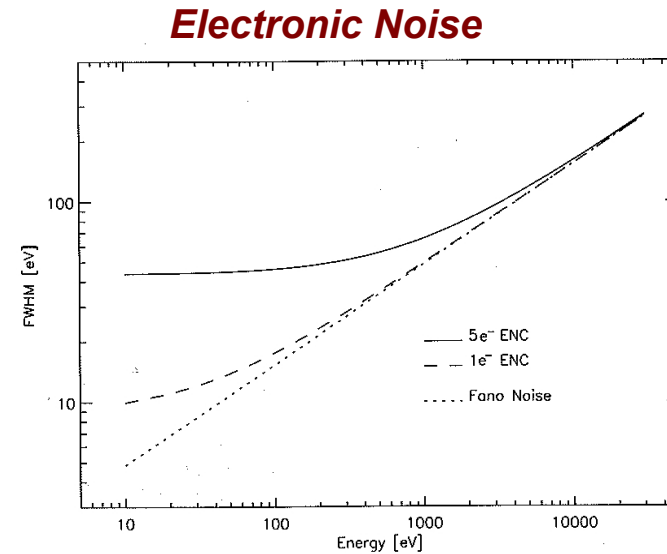
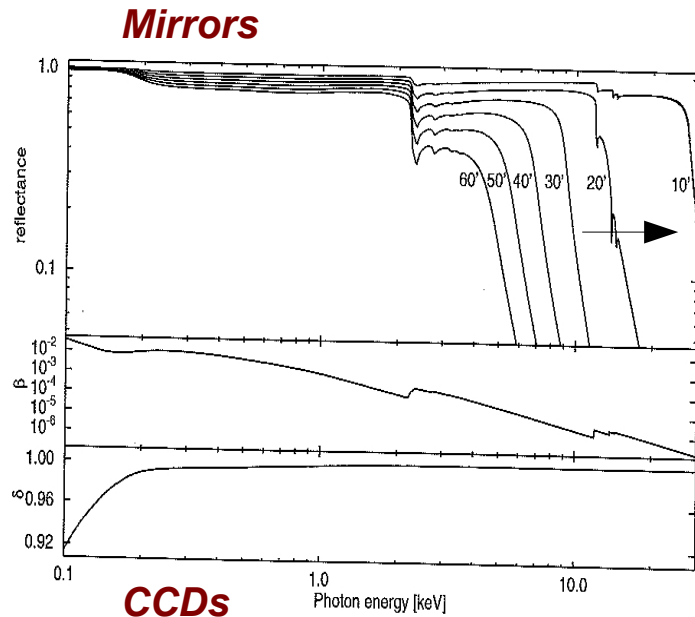
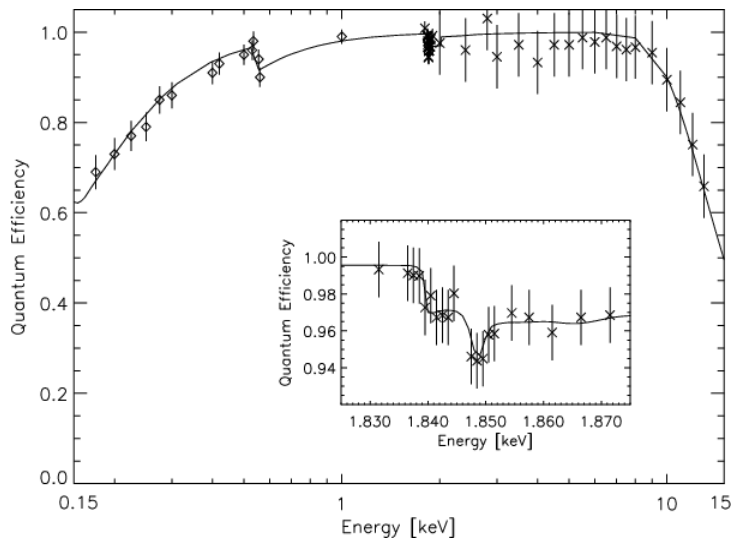


Fig. 7.8 Energy resolution as a function of the photon energy. The Fano noise is taken into account as well as a $5 e^-$ and $1 e^-$ electronic equivalent noise charge (ENC_{el}), respectively [22]



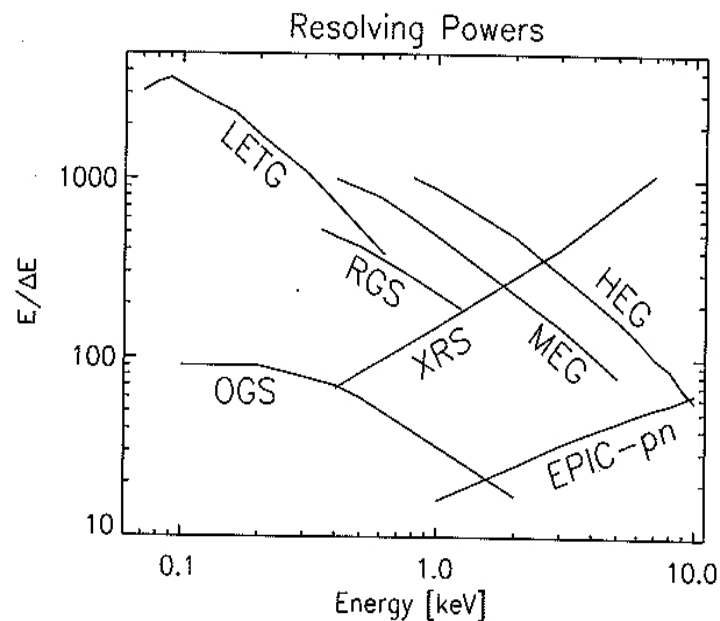
IPC - 400 eV @ 1 keV
 CCD - 100 eV @ 1 keV

Resolving power $E/\Delta E$:

- slightly degrades with E
- severely degrades towards lower energies !!!!!

Diffraction spectrometers – gratings:

Contrary to other energy bands, spectroscopy is performed with different instrument than photometry.

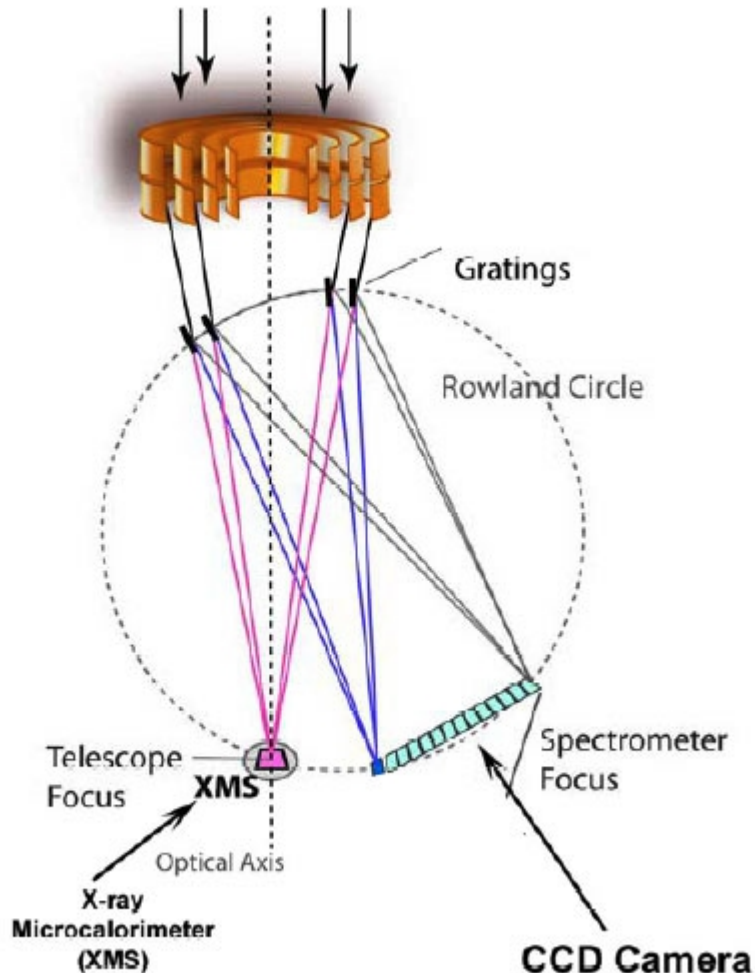


Transmission Gratings
on CHANDRA

Reflection Gratings
on XMM-Newton

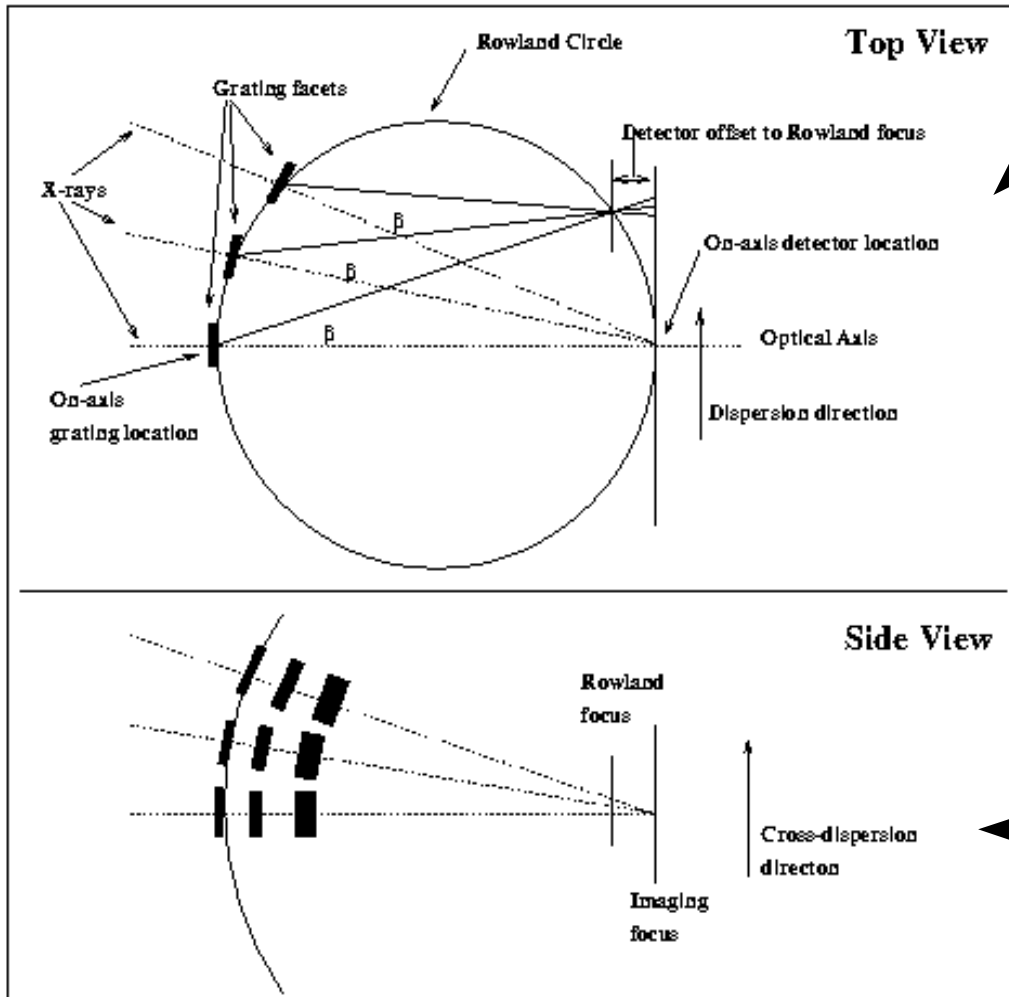
Fig. 8.1 Resolving power of various spectroscopic instruments (Einstein Observatory-OGS, Chandra Observatory-LETG, Chandra Observatory-HETG, XMM-Newton RGS, XMM-Newton EPIC pn-CCDs, Suzaku XRS)

Gratings placed into the beam path between the Wolter telescope and the focal plane, preferably close to the mirror exit.



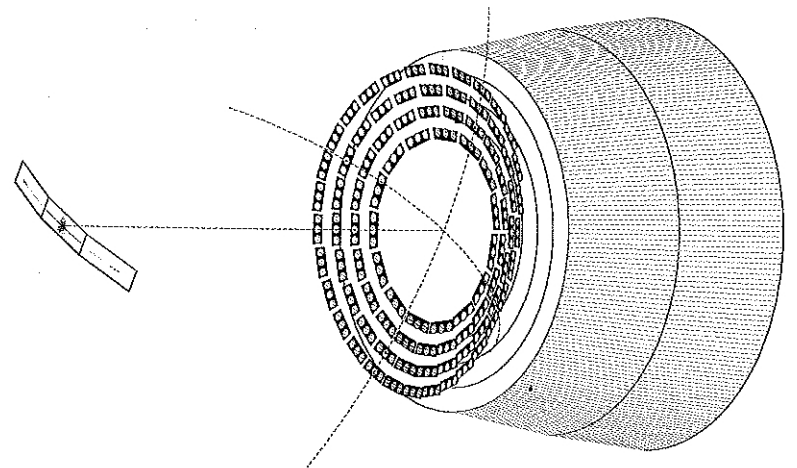
Grating ring is filed with little grating elements of two types: **transmission or reflection.**

Ring has to follow **Rowland Torus** to guarantee equal beam path for all rays.



We are looking across dispersion direction,
 dotted line – zero order
 solid line – first order,
 β - is diffraction angle.

We are looking along the dispersion direction.



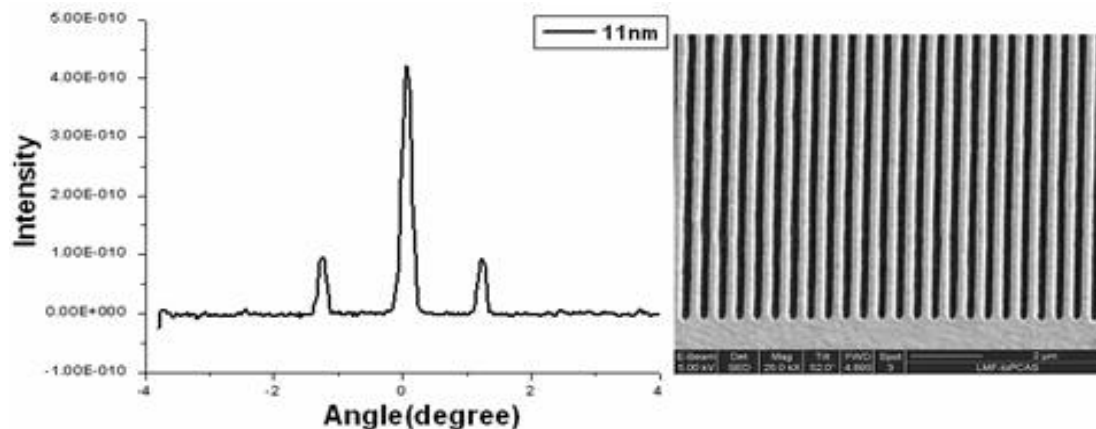
Resolution is given by:

Grating line density,
Angular resolution of the telescope.

The dispersion angle corresponding to a given wavelength , λ :

$$\sin \beta = m \lambda / d$$

where m – diffraction order
 d – grating spacing



Line density varies between: $5001 - 50001 \text{ mm}^{-1}$,
obtained by nanotechnology, a pitch of $25 \text{ }\mu\text{m}$.

Typical grating material is gold:

- well suited for electroforming process
- high Z, sufficient opacity even below $1 \mu\text{m}$.

The efficiency of classical amplitude grating for (bars completely opaque, slits completely transparent):

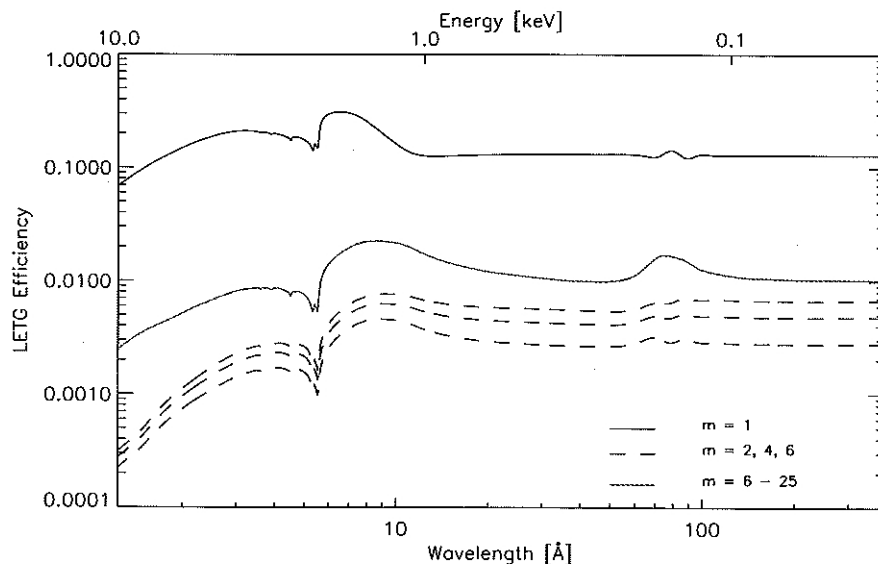


Fig. 8.4 Diffraction efficiencies of the Chandra Observatory LETG for first to sixth and sum of all higher diffraction orders. The design of the grating (bar/slit ratio = 0.5) suppresses the even (2nd and 4th) orders. With a thickness of $\approx 0.4 \mu\text{m}$, the grating bars are partially transparent, and constructive interference enhance the efficiency at the Au-M edge below 10 \AA . Source: Chandra Proposer's Guide [14]

$$\frac{I}{I_0} = \frac{\left(\sin m \frac{a}{d} \pi \right)^2}{(m \pi)^2}$$

where a – slit width between grating bars.
 Ideal case when maximum efficiency for the first symmetric orders:

$$\frac{a}{d} = 0.5 \qquad \frac{1}{\pi^2} = 10.1\%$$

OGS – Objective transmission gratings on EINSTEIN
SRON Utrecht/ Netherlands.

Two gratings with densities 500, 1001 mm⁻¹.

They did not follow Rowland curvature, therefore:

$$E / \Delta E \leq 50$$

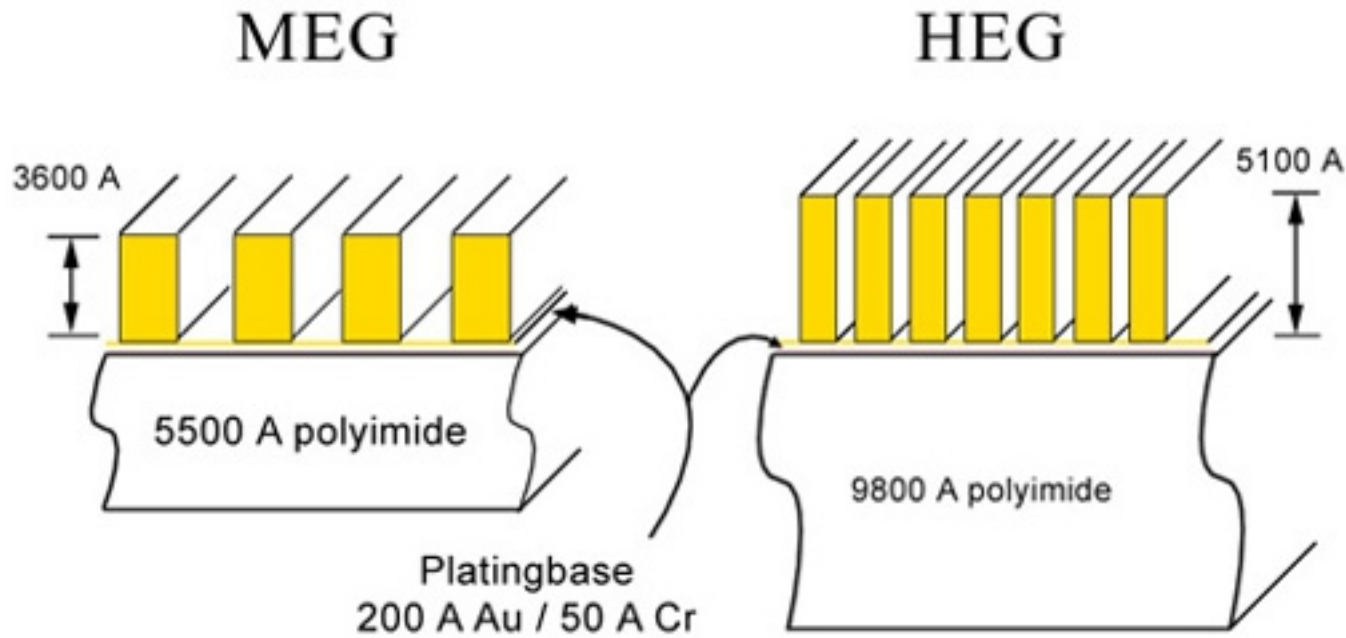
$$A_{eff} = 3 \text{ cm}^2 \quad @ \quad 44 \text{ \AA}$$

TGS – Transmission grating spectrometer on EXOSAT
SRON Utrecht/ Netherlands.

Two gratings with densities 5001, 10001 mm⁻¹.

$$A_{eff} = 10 \text{ cm}^2 \quad @ \quad 100 \text{ \AA}$$

CHANDRA has the best angular resolution, which implies **highest spectral resolution ever build so far.**

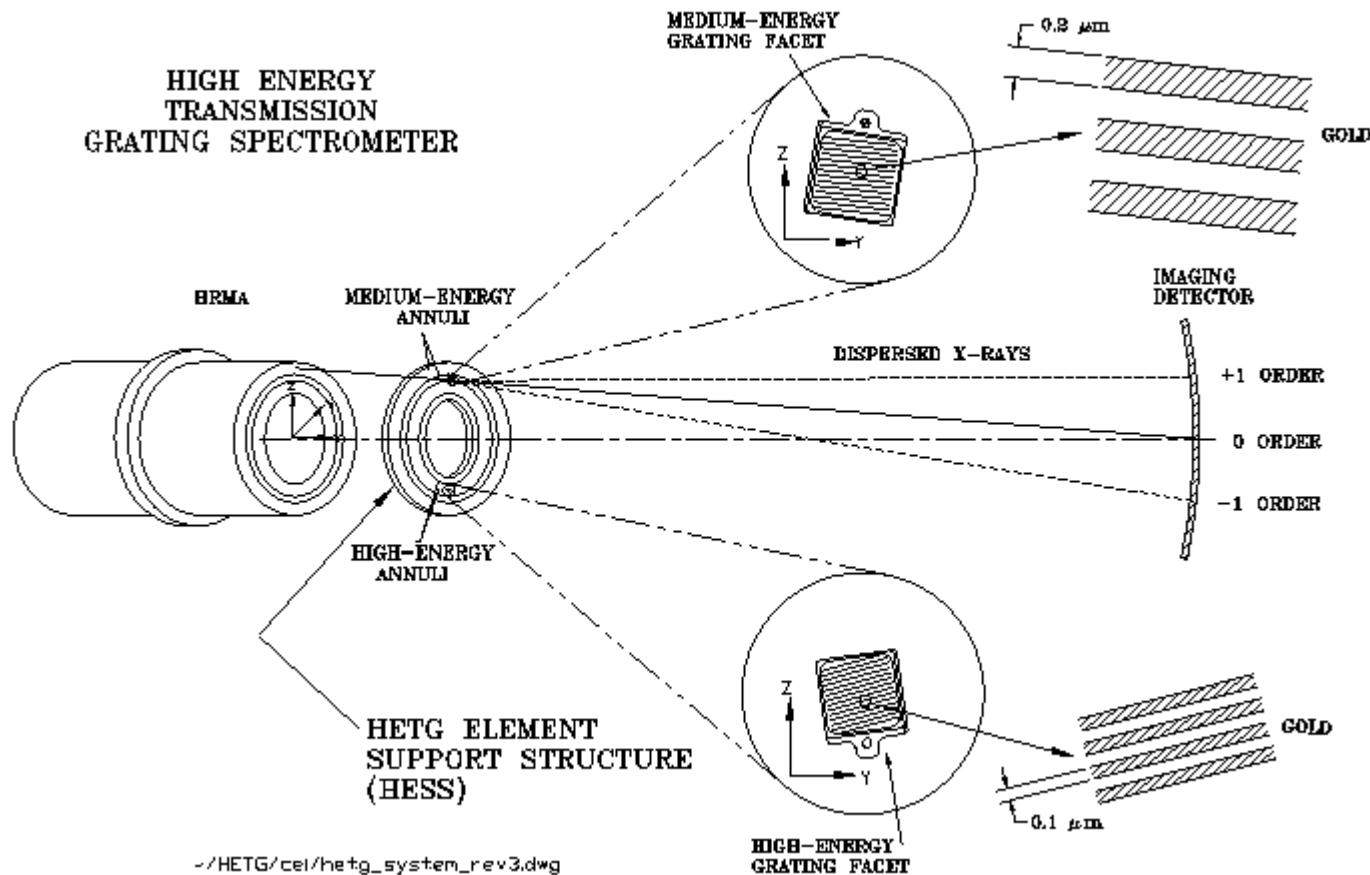


METG – 0.4-5 keV
25001 mm⁻¹,

HETG – 0.8-10 keV
50001 mm⁻¹

Two sets on single support structure, HETG comprise 336 grating elements in total.

HETG has been provided by MIT in Cambridge/USA.



METG – X-rays from outer mirror shells,
HETG – X-rays from inner mirror shells.
ACIS-S CCD detector.

LETG – 0.07-7 keV
50001 mm⁻¹,

540 elements,

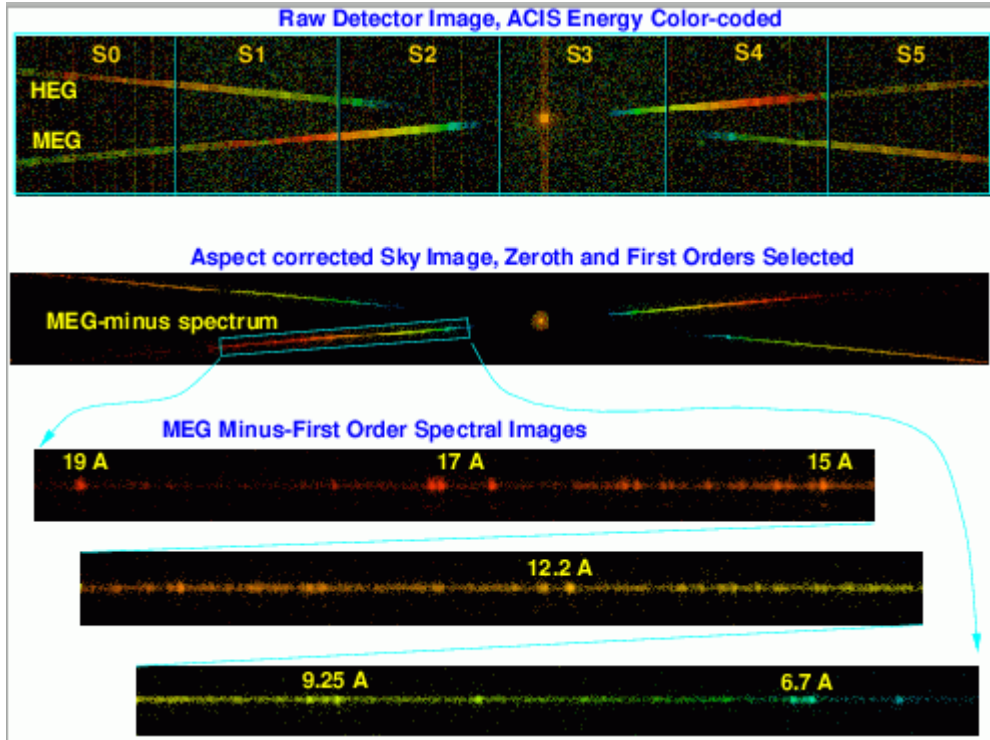
Highest resolving
power:

$$E/\Delta E \simeq 2000 \quad @ \quad 150 \text{ \AA}$$

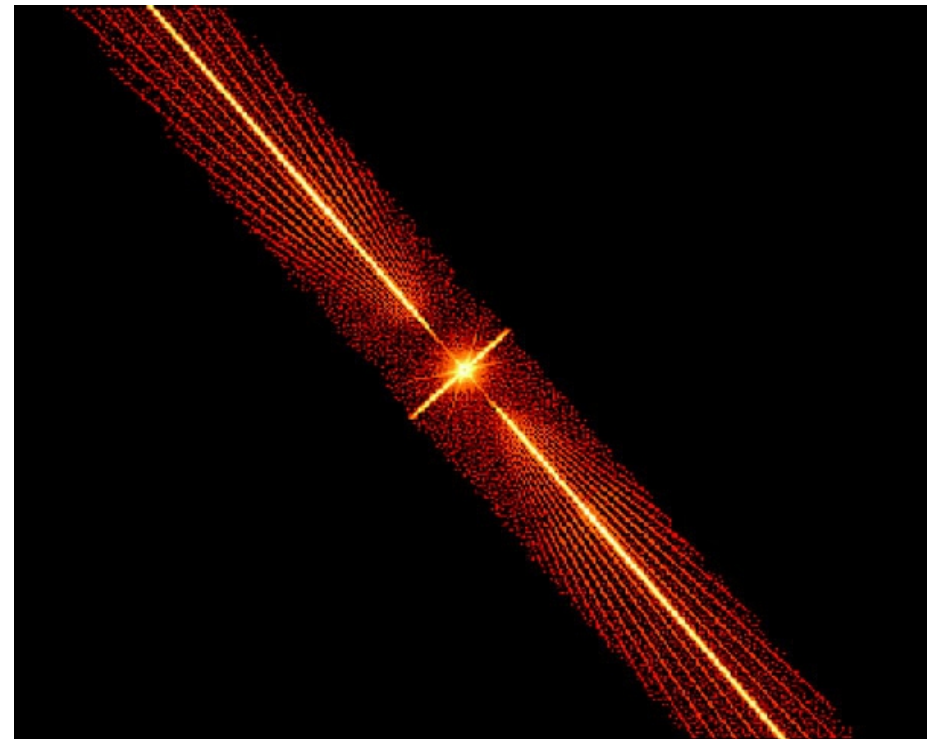


HRC-S – High Resolution Camera – microchannelplate detector sensitive to low energy photons, but does not provide energy resolution.

HETG ACIS-S



LETG HRC



RGS -Reflection grating spectrometer on XMM-NEWTON,
 their ruling density can be much lower since they
 are operating under shallow angles.

$$E / \Delta E \leq 600$$

$$A_{eff} = 260 \text{ cm}^2$$

Gratings
 are not
 parallel.

Highest effective area ever achieved.

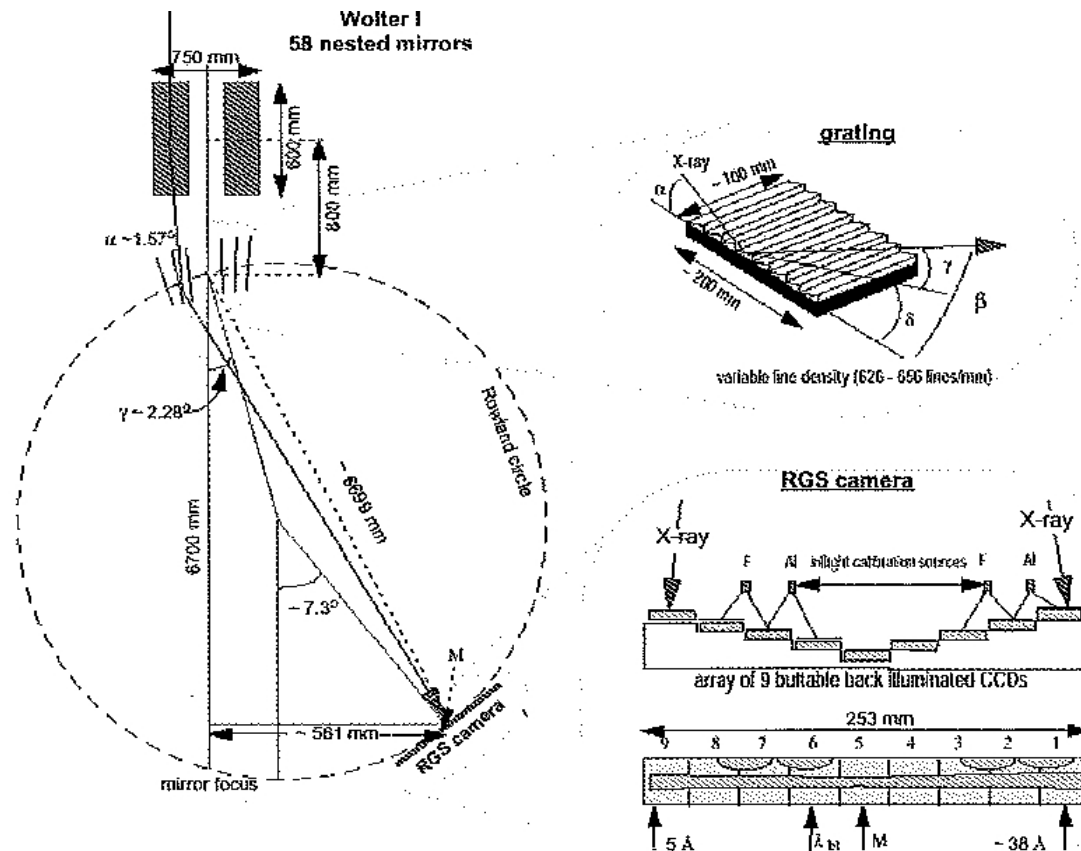
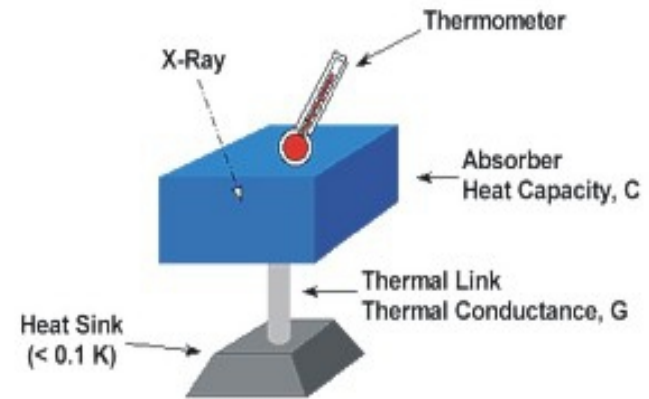


Fig. 8.9 RGS instrument [3]

Micro-calorimeters – Bolometers:

Microcalorimeter is a type of X-ray detector which consists of an X-ray absorber, a sensitive thermometer and a weak link to a thermal bath.

X-ray photon is converted into heat, thus raising the temperature of the absorber.



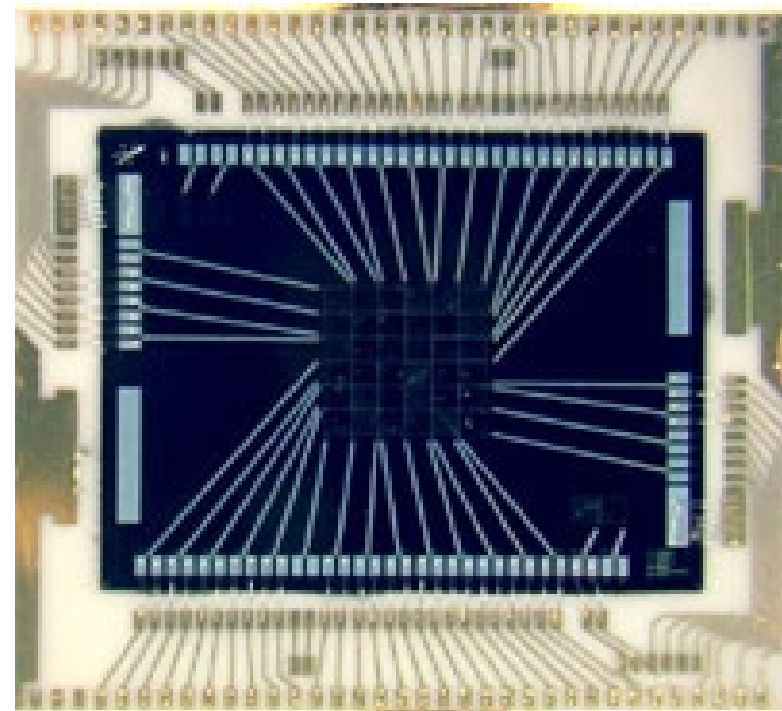
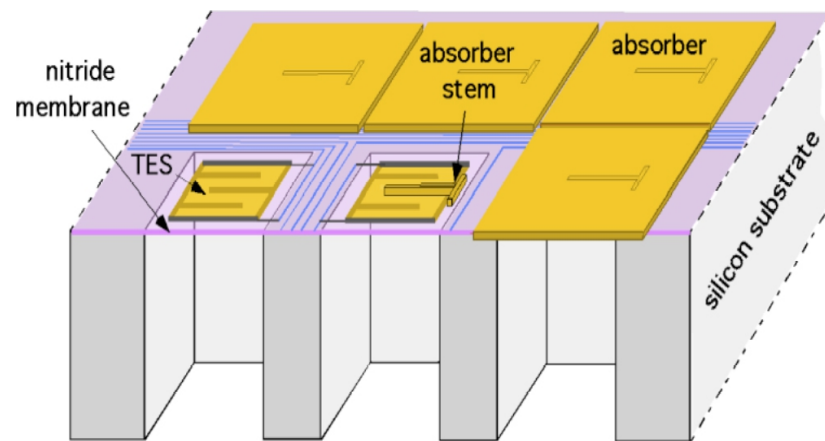
By measuring the amount of heat we are measuring the energy of the X-ray. Desirable absorber properties include low heat capacity (to magnify the temperature rise and high quantum efficiency).

The weak link cools the device after photon absorption to reset it for the next photon.

Thermodynamic noise associated with this link makes microcalorimeters work best at cryogenic temperatures.

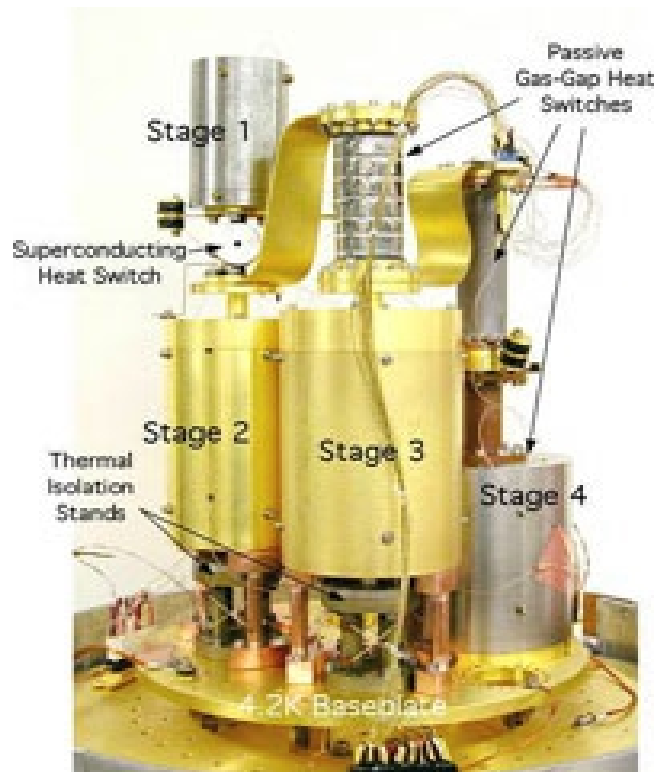
Several thermometer technologies are under development.

Superconducting technology – the transition edge sensor (TES).



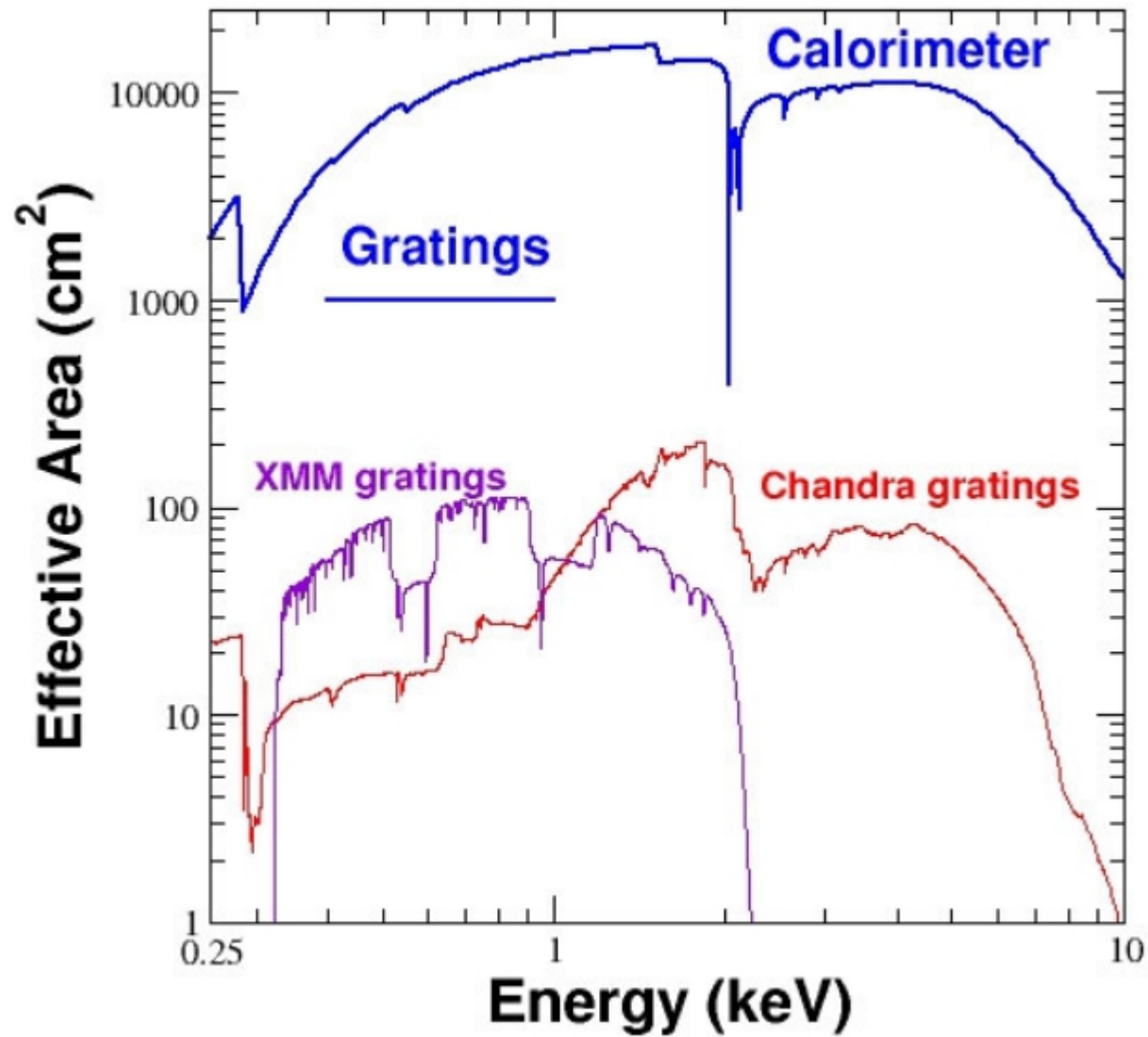
Microcalorimeters are operated in the narrow temperature range between the onset of non-zero resistance and the fully normal state.

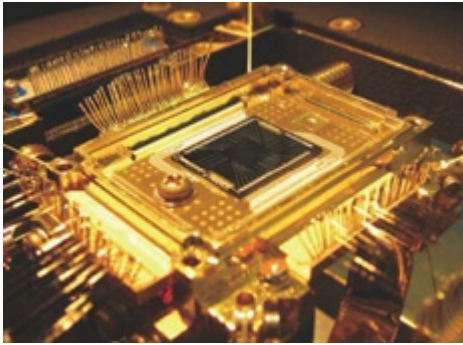
Three steps in cooling : 1) solid neon
2) liquid helium
3) adiabatic demagnetization refrigerator



SUZAKU lost of its helium just after lunched in June 2005.

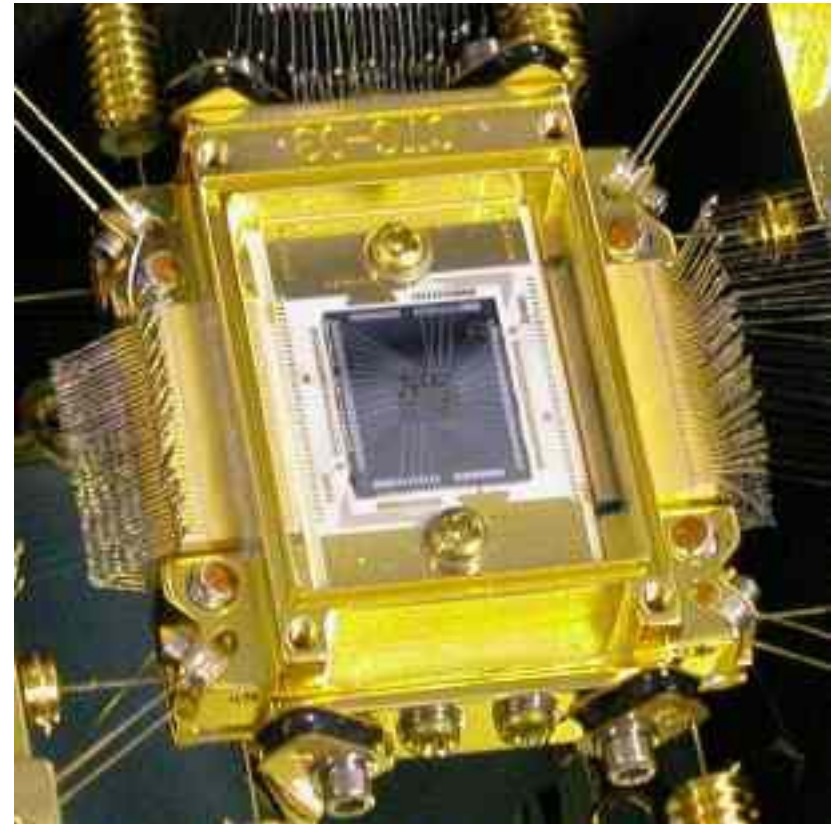
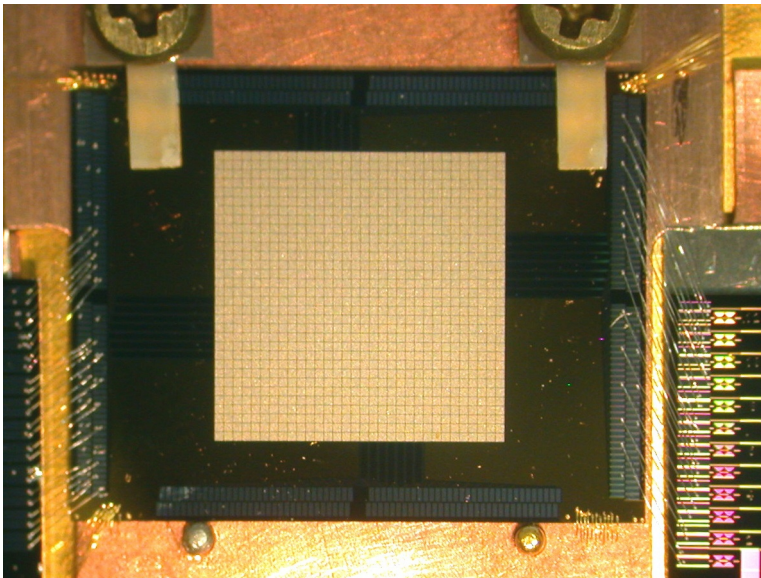
Predicted effective area for calorimeter.





SUZAKU, ASTRO-H, IXO

Microcalorimeter array:



JAXA three times tried to build micro-calorimeter:

2000 – ASTRO-E has been lost in the ocean during launch.

JAXA three times tried to build micro-calorimeter:

2000 – ASTRO-E has been lost in the ocean during launch.

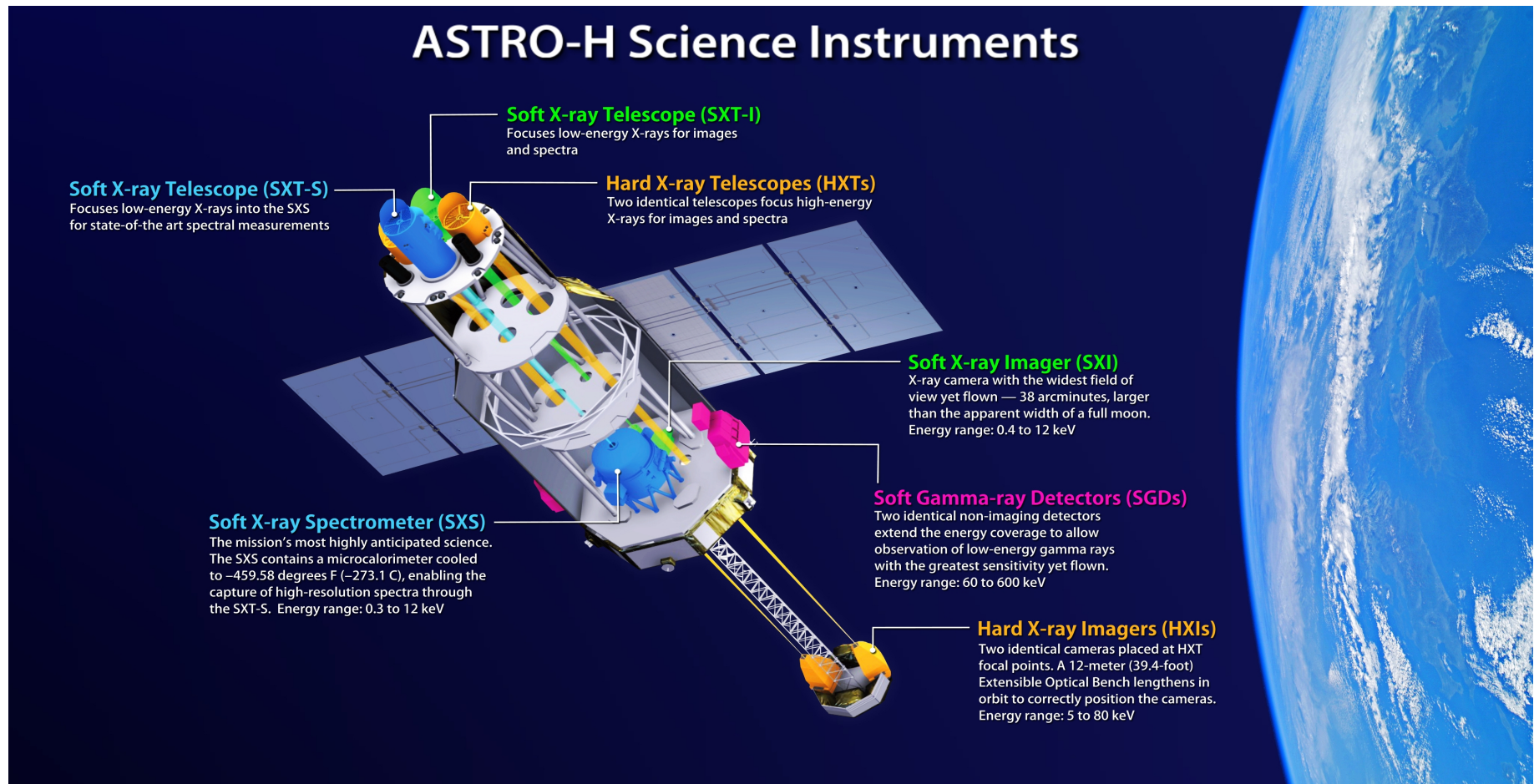
2005 – SUZAKU (ASTRO-EII) has lost all liquid helium, and micro-calorimeter does not work.

JAXA three times tried to build micro-calorimeter:

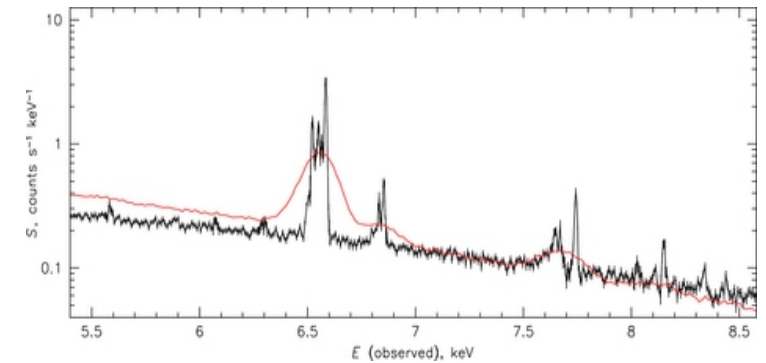
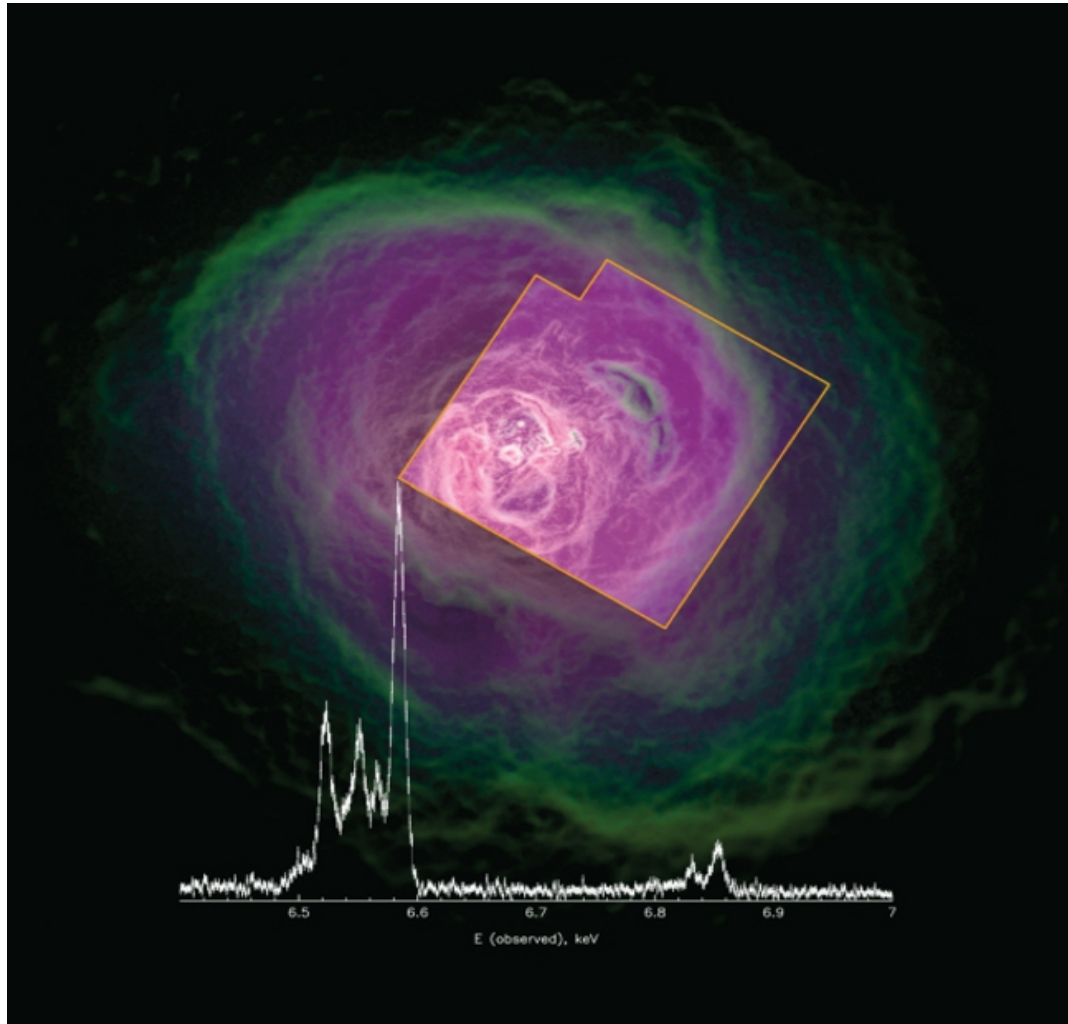
2000 – ASTRO-E has been lost in the ocean during launch.

2005 – SUZAKU (ASTRO-EII) has lost all liquid helium, and micro-calorimeter does not work.

2016 – ASTRO-H, launched on Feb. 2016, renamed as HITOMI, lost on March 2016 due to the software mistake.



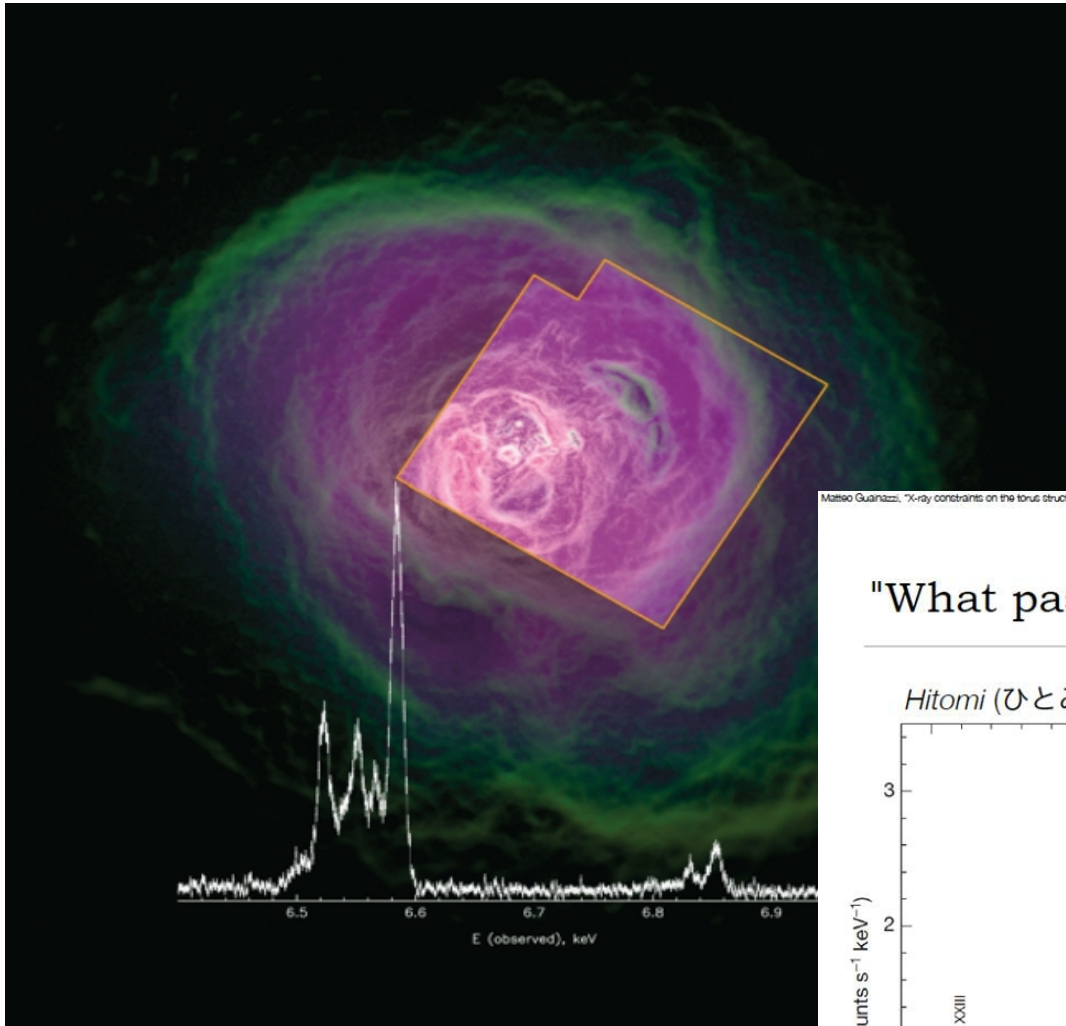
**HITOMI team NATURE paper issued at July 2016:
- emission from Perseus galaxy cluster with lines !!!**



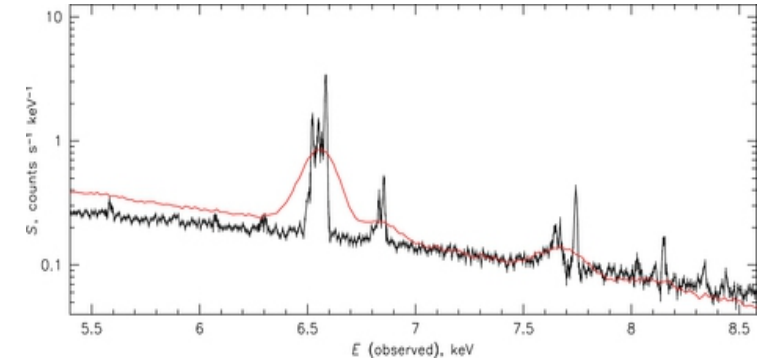
Comparison with SUZAKU

Emission triplet from helium-like Fe ions.

HITOMI team NATURE paper issued at July 2016: - emission from Perseus galaxy cluster with lines !!!



Emission triplet from helium-lil



Comparison with SUZAKU

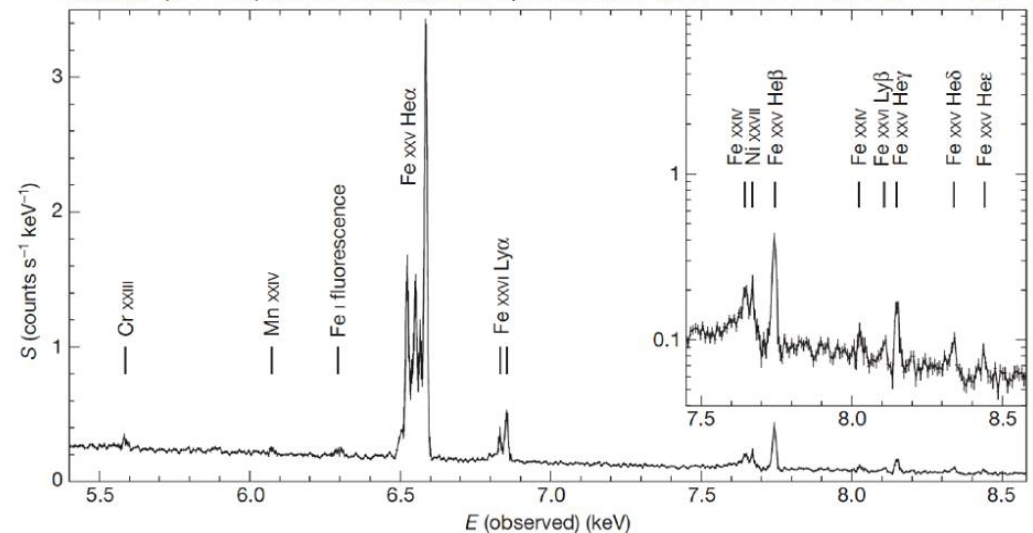
Matteo Guainazzi, "X-ray constraints on the ionc structure", EVASS 2016, Athens 8 July 2016



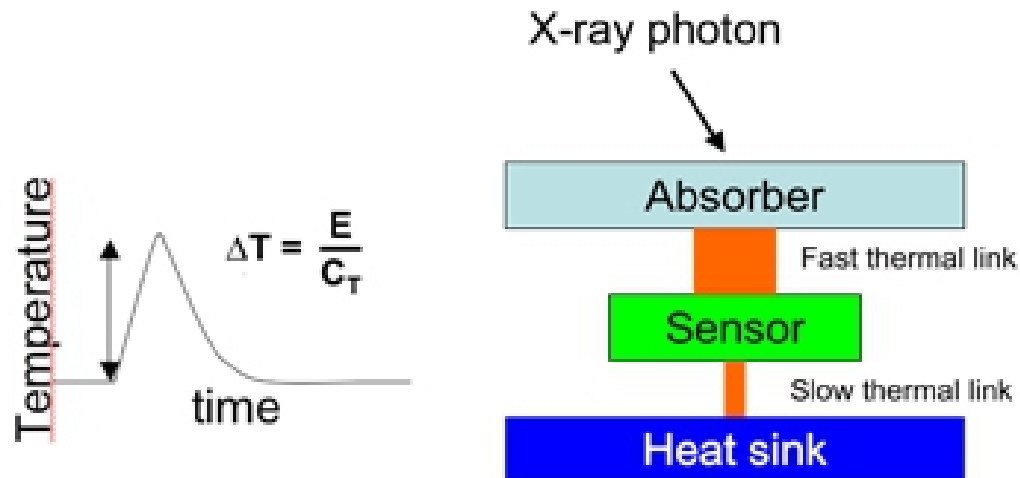
"What past is prologue." [W.Shakespeare, "The Tempest"]

Takanashi et al., 2016, Nature, in press

Hitomi (ひとみ) micro-calorimeter spectrum of the Perseus Cluster - 230 ks



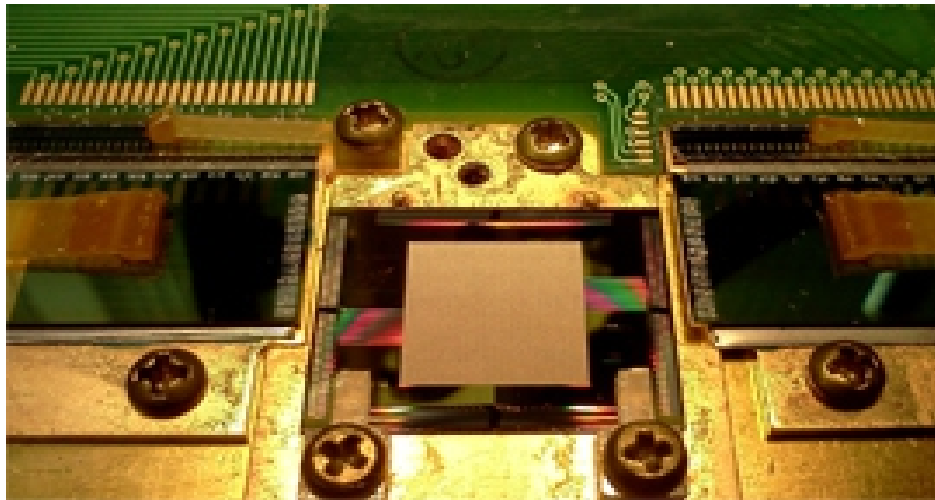
X-IFU – 0.3-12. keV is an array of **Transition Edge Sensors (TES)** working as micro-calorimeters



The absorption of an X-ray photon heats both the absorber and the sensor. The resulting signal represents the total energy deposited. The system goes back slowly to its original state through a weak thermal link with a heat sink.

X-IFU – 0.3-12. keV is an array of
Transition Edge Sensors (TES)
working as micro-calorimeters

TES Array – X-ray Microcalorimeter Spectrometer (XMS)

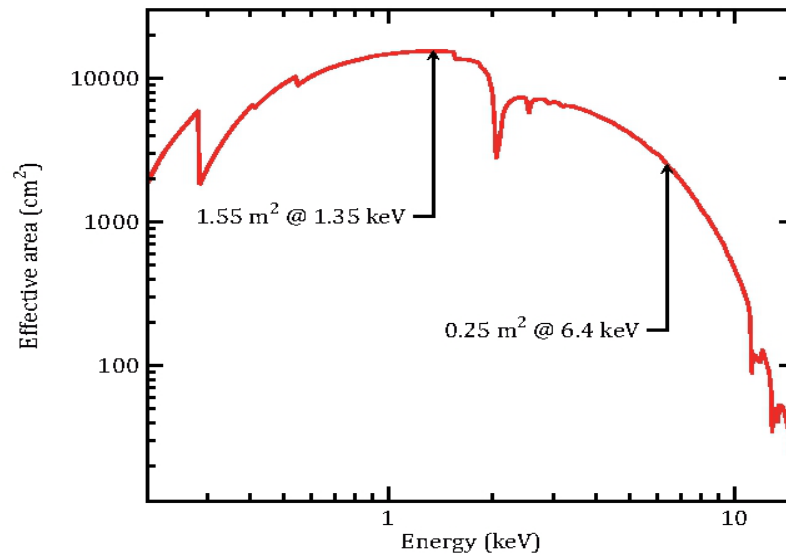
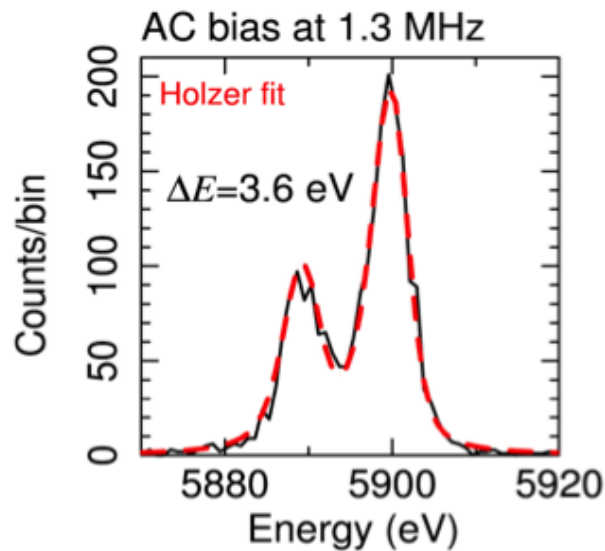


The detector consists of an array of 3840 absorbers,
limited FoV - 5' x 5' (goal is 7' x 7')

Count rate capability – 1 mCrab point source
with 90% , high-resolution events

X-IFU – 0.3-12. keV is an array of **Transition Edge Sensors (TES)** working as micro-calorimeters

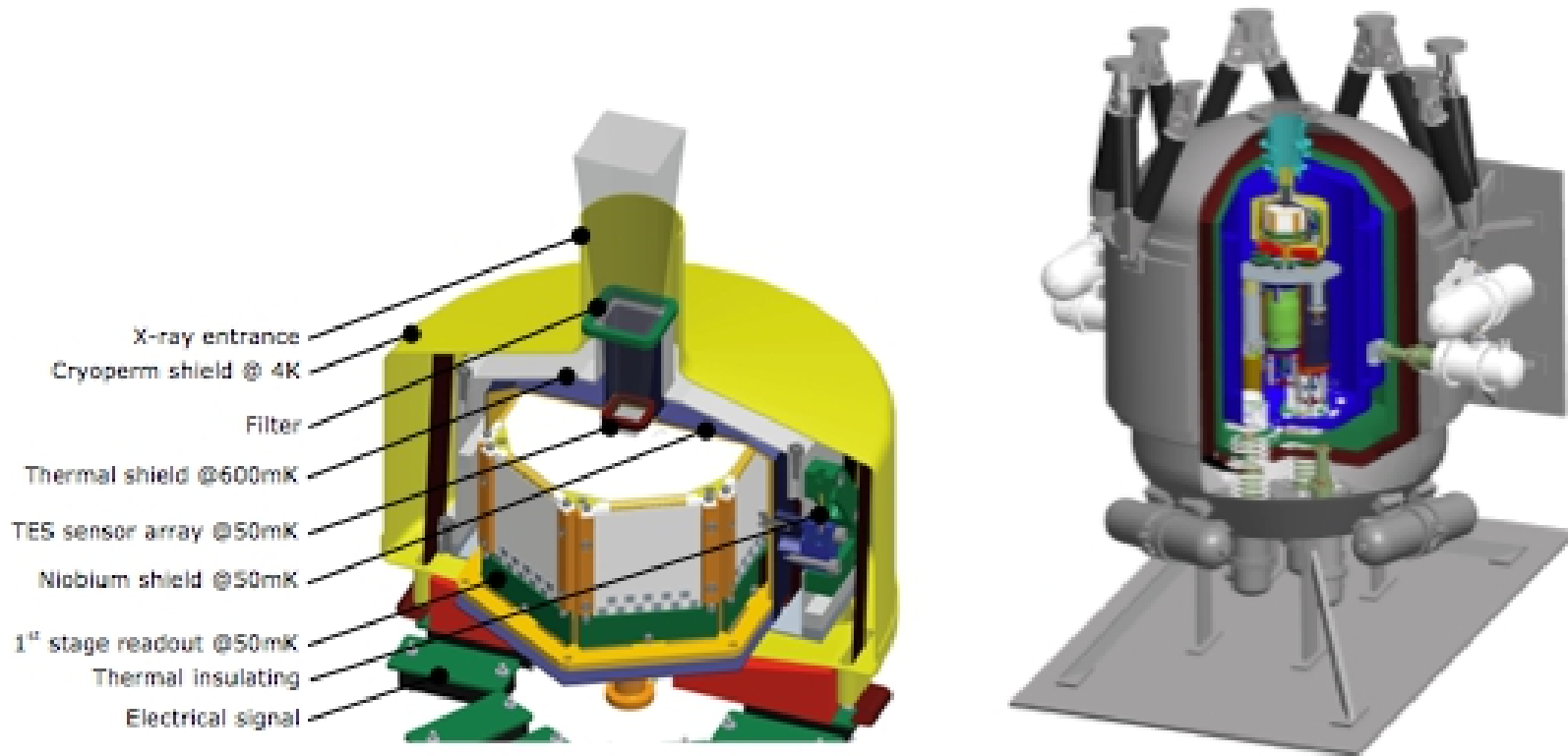
TES Array – X-ray Microcalorimeter Spectrometer (XMS)



The detector consists of an array of 3840 absorbers, limited FoV - 5' x 5' (goal is 7' x 7')

Count rate capability – 1 mCrab point source with 90% , high-resolution events

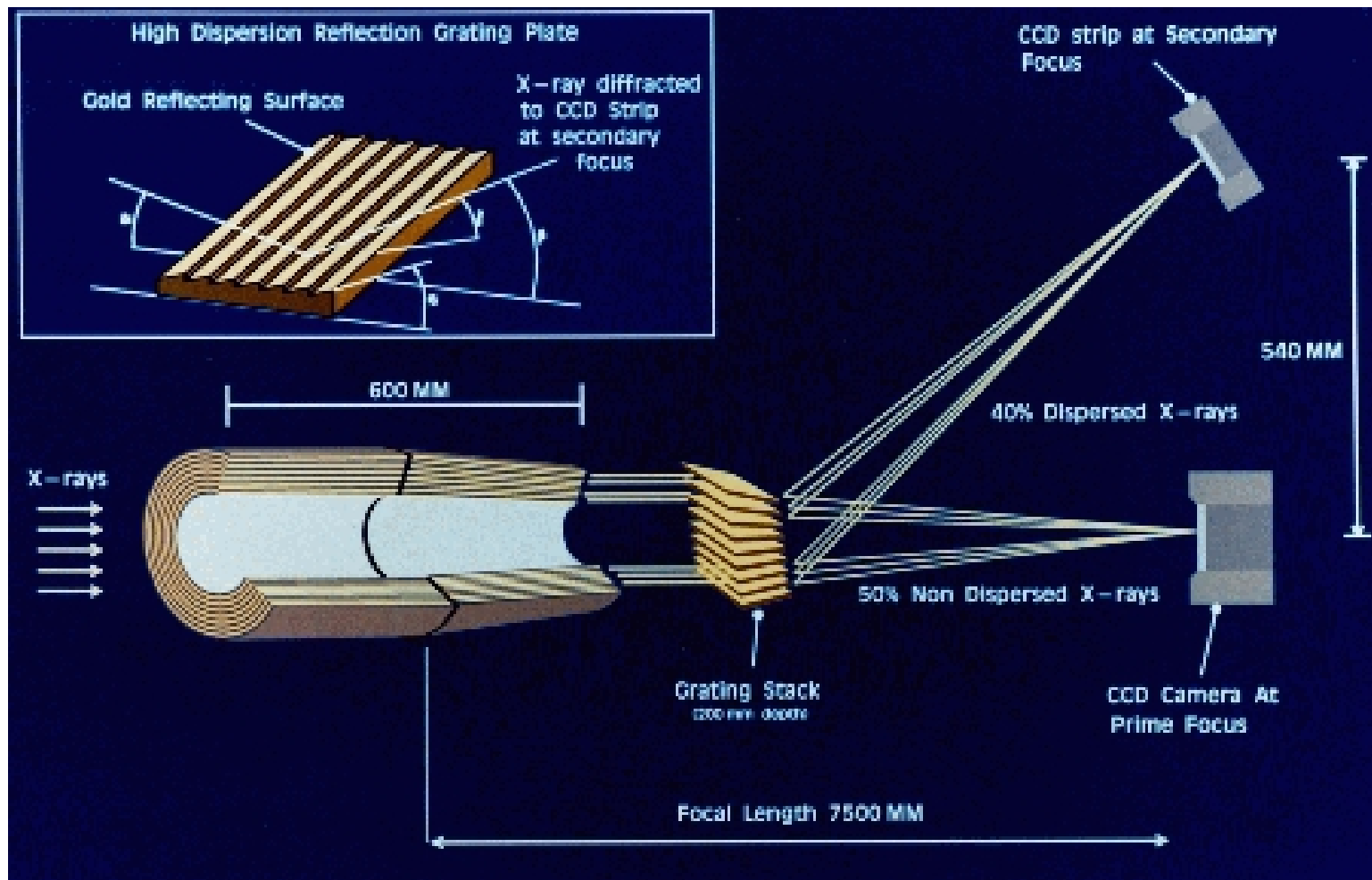
X-IFU – 0.3-12. keV is an array of **Transition Edge Sensors (TES)** working as micro-calorimeters



The sensor is coupled to a 50 mK bath. The instrument life time will not be limited by consumables as a combination of different, cryogen free, cooling techniques will be used.

Homework #4: find $A_{\text{eff}}(E)$, A_{eff} (off-axis angle), PSF for following gratings + mirrors + detector:

EINSTAIN, EXOSAT, ASCA, CHANDRA (LEG, HEG), XMM RGS, SUZAKU, HITOMI



Next steps:

- Overview of HW#1
- Lecture #5 – observations and hands-on sessions

**HOMEWORK #4: A_{eff} (E), A_{eff} (off-axis angle), PSF
EINSTAIN, EXOSAT, ASCA, CHANDRA (LEG, HEG),
XMM RGS, SUZAKU, HITOMI, eROSITA**

I will send you the table assigned for your name.

NEXT LECTURE on Dec. 1st 2022

wi-fi password: a w sercu maj

We have **eduroam** as well